

A study of abrasion in steel during comminution

Jean-Philippe Lafleur

Department of Mining and Materials Engineering

McGill University, Montreal

February 2011

A thesis submitted to McGill University in partial fulfillment of the requirements
of the degree of Master in Engineering

©Jean-Philippe Lafleur 2011

Abstract

Comminution is a process used in mineral processing for the size reduction of mined material, to permit effective handling, separation and recovery. The equipment used is kinetically complex, with very high-energy impacts and high forces, leading to great amounts of abrasive wear. It is desired to develop a better understanding of these processes, to both measure them and increase comminution while reducing wear. The Steel Wheel Abrasion Test is a laboratory technique used to generate controlled, abrasive three-body wear. By altering the applied force, rotational speed of the wheel and abrasive agent used in the SWAT, the wear behaviour of a material can be quantified. High-stress wear, which occurs when abrasive material is degraded during the test, can replicate the processes occurring in comminution systems.

This work has found that abrasive wear will increase with increasing input energy into the tribological interaction. This wear can be linked to the energy input into the system, through the measurement of applied forces, wheel rotational speed and generated torque. This results in the development of a specific abrasion energy, E_{AS} , which provide an energy metric for the abrasion process. Furthermore, the breakage induced in the abrasive particles can also be quantified and evaluated, generating a comminution metric, the specific comminution energy, E_{CS} . These indices can then be linked, to develop an understanding of systems where comminution and abrasion occur concurrently.

Résumé

La comminution est un procédé utilisé dans l'industrie minéralurgique pour la réduction de taille d'un minerai, afin de permettre le transport, la séparation, la récupération et l'extraction de ce matériel. L'équipement utilisé pour cette tâche est complexe, soumis à des forces élevées et des impacts violents, ce qui génère une quantité importante d'usure. Une plus grande connaissance des processus de comminution et d'usure est nécessaire pour pouvoir évaluer leur amplitude, dans le but de favoriser la comminution tout en minimisant l'usure. Le test d'abrasion par roue d'acier (SWAT) est une technique de laboratoire utilisée pour générer de l'usure abrasive à trois composantes. En contrôlant la force appliquée, la vitesse de rotation de la roue et l'agent abrasif employé lors du test SWAT, il est possible d'évaluer la réponse d'une surface à l'abrasion. L'usure de haut stress, générée dans les systèmes où les agents abrasifs sont fracturés, peut répliquer les procédés présents dans l'équipement de comminution.

Ce projet a trouvé que l'usure abrasive augmente avec une augmentation de l'énergie investie dans l'interaction tribologique. Cette usure peut être liée à l'énergie du système, en mesurant les forces appliquées, la vitesse de rotation de la roue et la torsion générée. Ces valeurs peuvent être utilisées pour calculer une valeur spécifique d'énergie d'abrasion, E_{AS} , qui agit comme indice pour le procédé d'abrasion. De plus, la fragmentation créée dans les particules abrasives peut être évaluée, pour générer un indice de comminution, E_{CS} , l'énergie spécifique de comminution. Ces deux indices peuvent être liés, pour rejoindre les procédés de comminution et d'abrasion.

Acknowledgements

I would like to acknowledge the invaluable support and assistance of the many people who have made this research possible.

First, I extend my gratitude to Prof. Peter Radziszewski, who has taken me into to his research group and provided me with interesting research opportunities and invaluable advice. I would also like to thank Prof. James Finch, for agreeing to supervise me during my tenure as a graduate student.

The members of the Comminution Dynamics Laboratory have been essential to this work. Dr. Tapiwa Chenje has been an invaluable help, a source of advice, assistance and support. My other colleagues, Poorya Hosseini, Dr. Amar Sabih and David Hewitt, have also been of great assistance. I am grateful to have worked with them.

This work, and I, owes a great deal to the priceless contribution of the technical personnel of the Faculty of Engineering. Raymond Langlois and Monique Riendeau of the Department of Materials Engineering were of great help throughout this effort. Without the help of Gary Savard, John Boisvert and Raymond Lemay, of the Department of Mechanical Engineering, this work could not have been possible. Their technical support, equipment troubleshooting and emergency repairs kept the lab functioning and my sanity relatively intact.

Finally, I would like to thank my family for their love and support. They have been there, through thick and thin. I am more grateful than I can ever express.

Table of Contents

Abstract.....	i
Résumé.....	ii
Acknowledgements.....	iii
Table of Contents.....	iv
List of Figures.....	vi
List of Tables.....	vii
Chapter 1 Introduction.....	1
1.1 Motivation.....	2
1.2 Objectives.....	3
Chapter 2 Literature Review.....	4
2.1 Mineral Processing and Comminution.....	5
2.1.1 Introduction.....	5
2.1.2 Particle breakage.....	6
2.1.3 Comminution equipment.....	8
2.1.4 Comminution models.....	15
2.2 Wear.....	16
2.2.1 Introduction.....	16
2.2.2 Adhesion, fatigue and erosion.....	17
2.2.3 Abrasion.....	21
2.2.4 Corrosion.....	33
2.3 Abrasion modeling and measurement.....	35
2.3.1 Introduction.....	35
2.3.2 Rubber Wheel Abrasion Test.....	37
2.3.3 Ball Mill Abrasion Test.....	38
2.3.4 Steel Wheel Abrasion Test.....	39
2.3.5 Decoupled wear model.....	41
2.4 Degradation mitigation in comminution equipment.....	44
2.5 Summary.....	45
Chapter 3 Methodology.....	46
3.1 Introduction.....	47
3.2 Steel wheel abrasion test.....	47
3.3 Material selection.....	50
3.4 Experimental parameters.....	52
3.5 Test identification and nomenclature.....	53
3.6 Experimental procedure.....	54
3.7 Particle size determination.....	55
3.8 Torque data processing.....	56
3.9 Experimental methods modifications.....	56
3.10 Summary.....	57
Chapter 4 Results and Discussion.....	58
4.1 Wear scar characterisation and analysis.....	59
4.2 Wear as mass loss response.....	64
4.3 Specific abrasion energy.....	69

4.4	Specific comminution energy	74
4.5	Linking comminution and abrasion specific energies	81
4.6	Effect of wheel rotational speed	85
4.7	Analysis of material type performance	85
4.8	Summary	87
Chapter 5	Conclusion	88
5.1	Conclusion	89
5.2	Recommendations.....	91
5.3	Final statement.....	94
References	95

List of Figures

Figure 2-1: Breakage modes; R1 compression, R2 shear, R3 impact (stroke), R4 impact (collision) [2]	6
Figure 2-2: Ball Mill [1].....	10
Figure 2-3: Mill charge motion: (a) cascading, (b) falling, (c) centrifugal [2]	11
Figure 2-4: Mill charge profile [11]	12
Figure 2-5: Adhesive surface interaction [22].....	18
Figure 2-6: Abrasive wear mechanisms [25]	22
Figure 2-7: Ploughing, steel pin against brass [26]	23
Figure 2-8: Wedge formation, steel pin against stainless steel [26]	24
Figure 2-9: Cutting, steel pin on brass [26].....	24
Figure 2-10: Abrasive system configuration [22]	27
Figure 2-11: Abrasive system configuration, (a) open two-body, (b) closed two-body, (c) open three-body, (d) closed three-body [25].....	28
Figure 2-12: Wear rate as determined by relative hardness ratio between surface and abrasive agent [24].....	30
Figure 2-13: Rabinowicz's abrasive wear model [37].....	35
Figure 2-14: ASTM G65 Dry Sand Rubber Wheel test[43]	37
Figure 2-15: Wear scar schematic[34].....	41
Figure 2-16: SWAT wheel free body diagram[39]	43
Figure 3-1: SWAT apparatus, Version 3 (left) CAD design, (right) apparatus	47
Figure 3-2: SWAT Sample application system and force diagram[56]	48
Figure 3-3: Sample torque voltage graph, test D32-30-150-2.....	56
Figure 4-1: Sample B32-20-150-1.....	59
Figure 4-2: Sample A32-20-90 wear scar, top view, 2X magnification	60
Figure 4-3: Sample A32-20-90, bottom view, 2X magnification	60
Figure 4-4: Sample D71-20-90-2	61
Figure 4-5: Sample A32-20-210, 2X magnification, digitally stitched.....	61
Figure 4-6: Sample A32-20-210, Middle view, 3X magnification	62
Figure 4-7: Sample A32-20-210, Side view, 3X Magnification	63
Figure 4-8: Mass loss in wear as a function of applied force, 1018 Steel	65
Figure 4-9: Mass loss in wear as a function of applied force, 150 RPM, Barco 32 abrasive	66
Figure 4-10: Mass loss in wear as a function of applied force, 150 RPM, Barco 71 abrasive	66
Figure 4-11: Mass loss in wear as a function of work input	68
Figure 4-12: Specific abrasion energy as a function of applied force, 1018 steel	70
Figure 4-13: Specific abrasion energy as a function of applied force, 150 RPM, Barco 32 abrasive	71
Figure 4-14: Specific abrasion energy as a function of applied force, 150 RPM, Barco 71 abrasive	72
Figure 4-15: Specific comminution energy as a function of applied force, 1018 steel.....	76
Figure 4-16: Percent passing a given particle size, 1018 steel, 150 RPM	78
Figure 4-17: Specific comminution energy as a function of applied force, 150 RPM, Barco 32..	79
Figure 4-18: Specific comminution energy as a function of applied force, 150 RPM, Barco 71..	81
Figure 4-19: Specific comminution energy vs. specific abrasion energy, Barco 32	82
Figure 4-20: Specific comminution energy vs. specific abrasion energy, Barco 71	82
Figure 4-21: Specific comminution energy vs. specific abrasion energy, curve fitting.....	84

List of Tables

Table 2-1: Size reduction stages [4]	8
Table 3-1: Abrasive material size distribution by percentage	50
Table 3-2: Steel test material elemental composition ranges	51
Table 3-3: Steel sample hardness values	52
Table 4-1: Specific abrasion energy values for B32 and C32 systems	74
Table 4-2: Applied force, torque and specific comminution energy, 150 RPM tests	80
Table 4-3: Specific energy potential schema	83

Chapter 1 Introduction

1.1 Motivation

Modern civilisation has a near limitless appetite for the resources required to maintain the current human population and continue further technological and economic development. The mining and mineral processing industry is tasked with the effective and economical extraction of the metals and minerals required to meet this need for raw materials. In all the techniques and processes used, there exists a requirement that the resources, first extracted as raw materials, be successfully transformed into a usable end product. This processing often requires that the material be crushed or ground down to a usable size. Comminution, the technical term for particle size reduction, requires the deployment of specialized, complex and expensive equipment. Energy demands are elevated. The conditions in which this equipment operates are universally harsh and prone to high levels of wear and degradation. Failure is expensive, time consuming and potentially dangerous.

Comminution is energy intensive, estimated to account for approximately two percent of all global energy usage [1]. The intrinsic efficiency of the processes is often quite low, usually only a few percent [1]. In terms of cost, comminution can account for up to half of total operating costs for a mine. Tumbling mills, a common type of equipment, have large metal charges that wear out and must be replaced. In 2000, annual consumption of steel for these mills, in the United-States alone, was approximately 500 000 tons. The worn iron, released from the degraded steel, can also have deleterious impact on the other processes in the extraction circuit [1-5].

The Comminution Dynamics Laboratory, in the Department of Mechanical Engineering, at McGill University, Montreal, Canada, seeks to understand the process of comminution. This research group attempts to measure, model and quantify what occurs in comminution mills, both in terms of the particle breakage induced, which is the goal of comminution, and the undesired wear that occurs in these processes. In determining what occurs, it is hoped that these processes can be rendered more efficient and effective.

1.2 Objectives

The goal of the present work is to investigate a technique for abrasion resistance measurement, the steel wheel abrasion test (SWAT), and explore its applicability to comminution measurement. Using this test, it is hoped that comminution and abrasion can be experimentally measured concurrently. In reaching this goal, it will be necessary to:

1. Develop an understating of the process of comminution.
2. Develop an understating of wear and its component mechanisms.
3. Study the technique by which both of these processes can be replicated and measured effectively.
4. Develop metrics to measure the energy requirements of these processes.
5. Link these energy metrics, to find a connection between abrasive wear and comminution.

Chapter 2 Literature Review

The present section will review the scientific and technical literature needed to understand the processes of comminution and abrasion. Comminution will be studied to overview the topic of particle size reduction mechanisms, the equipment employed and some theoretical underpinnings. Wear will be studied with regards to the mechanisms that cause it, with particular emphasis on abrasion. Models of abrasion and research techniques used to study it will be addressed.

2.1 Mineral Processing and Comminution

2.1.1 Introduction

Mineral processing is the collection of techniques used in the transformation of mineral ores to generate concentrated products [1]. The goal of this processing is to transform a mined raw material, using a variety of physical and chemical techniques, into a usable end product. While the techniques will vary from material to material, given differences in deposit geology and mineralogy, extraction methods, processing equipment and operational requirements, the basics remain the same. There are four major steps: extraction, comminution, separation and concentration. Extraction is the process in which the ore is removed from the ore body itself, essentially, mined. Comminution is the process of reducing the size of the material, through crushing and grinding. The goals of comminution are threefold: liberating the desirable mineral from the ore, permitting effective material handling and increasing particle surface area for further chemical reactions [1]. Separation and concentration are the stages where the physical and chemical properties of the liberated particles are used to separate the desirable mineral from the undesirable gangue. Particles will be screened according to size and separated according to their density, floatability or magnetic properties.

The term comminution is used to describe the class of techniques employed in the size reduction of ore particles. Comminution occurs in multiple instances in mineral processes. Initial size reduction first occurs during the extraction stage, when ore is removed from the deposit, due to fracture caused by

explosive blasting or mechanical breakage caused by mining machinery. Ore is then directed to the mill for concentration, where it undergoes crushing and grinding in dedicated stages.

2.1.2 Particle breakage

Breakage of a particle occurs under a given set of conditions, detailed in Figure 2-1. The comminution event occurs when force is applied to the particle. This force may be caused by the action of an external agent impacting, compressing or shearing the particle, or through the impact of the particle itself against the size of the comminution equipment.

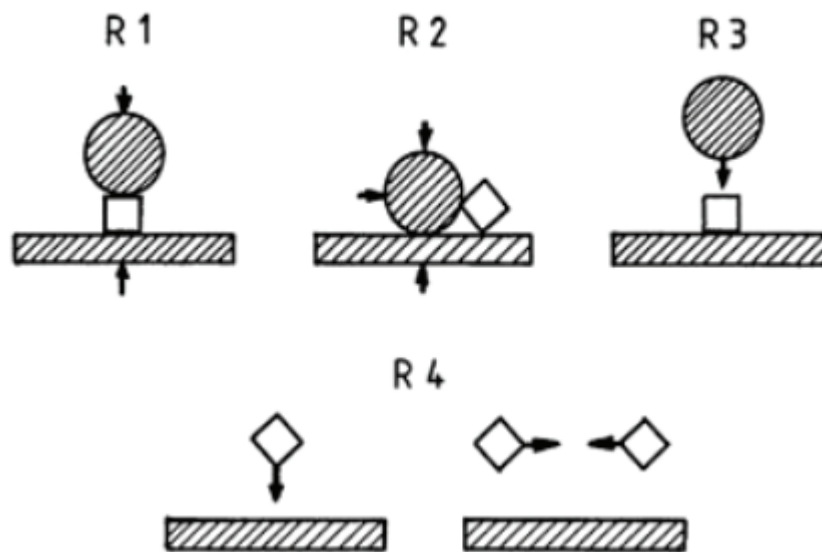


Figure 2-1: Breakage modes; R1 compression, R2 shear, R3 impact (stroke), R4 impact (collision) [2]

Particle breakage, while extensively studied, is still a complex phenomenon which is not entirely predictable [1]. When a particle is subjected to a force, the strength of that particle is determined as the stress at the point of initial fracture, as a force per unit area of particle cross-section, while the

breaking energy is the work done to a particle to fracture it [1]. The theoretical strength of a particle is usually on the order of a tenth to a twentieth of its modulus of elasticity. Actual material strength, however, is significantly less by a few orders of magnitude. As with all other material types, this difference is due to defects within the solid particles, which lower the strength of the material [1].

The theoretical yield strength assumes perfect material structure, free of all defects, voids, cracks and inhomogeneities. Flaws, such as cracks, will act to concentrate stresses and promote fracture at those locations. These flaws will reduce the energy needed to fracture the material [6]. Ore particles processed in comminution equipment are prone to these defects, due to the steps taken in their extraction [1]. Energy input into the breakage event will be used to create new surfaces for the fragments produced and in deformation of the material at the crack tips. After the breakage event, several product particles are created in a variety of size configurations. The breakage behaviour of a particle into fragments is a complex process, depending on the structure, composition and strength of the original particle, as well as the way in which cracks propagate within the particle. The size of the original particle will also influence energy requirements in fracture. It is well known that larger particles require less energy, on a proportional basis, to break than finer particles [7]. This is caused by a number of factors. There is a greater number of flaws in larger particles, which are depleted during breakage into smaller particles. Furthermore, larger particles have a higher probability of a caught and crushed than smaller particles [7]. As the product of a comminution process becomes finer, the energy requirements become greater and greater. The

situation becomes even more complex in systems where multiple particles, both in number and in type, are being broken simultaneously.

2.1.3 Comminution equipment

Equipment used in comminution is classified according to its size reduction range and method of action. The size reduction range provides the classification between crushing and grinding, and depends on the size of the material handled.

Table 2-1: Size reduction stages [4]

Size reduction step	Upper size	Lower size
Explosive shattering	Infinite	1 m
Primary crushing	1 m	100 mm
Secondary crushing	100 mm	10 mm
Coarse grinding	10 mm	1 m
Fine grinding	1 m	100 μm
Very fine grinding	100 μm	10 μm
Superfine grinding	10 μm	1 μm

The most basic division is between crushing and grinding equipment. Crushers function by compressing the ore particle between two surfaces, which exert a force on the particle and crush it down to a smaller size. The most common examples of these in industrial practice are the jaw crusher, cone crusher, gyratory crusher and roll crusher.

The jaw crusher operates using a fixed plate and a mobile plate with an oscillating motion. As ore is loaded into the top of the crusher, it moves down and is compressed with increasing force until breakage occurs. The largest size of

material produced is determined by the gap width of the discharge. Gyratory and cone crushers operate on a similar principle. They rely on a fixed surface and a moving surface, either gyrating or revolving, to compress the ore. Roll crushers use two fixed rolls, rotating towards each other. Material is loaded into the crusher and compressed between the rolls, leading to breakage. In these systems, comminution occurs primarily through compression [2].

Grinding equipment, at its most basic, consists of a hollow shell into which particles are loaded. The rotation of the shell leads to tumbling of the contents and size reduction of the particles. Common examples found in industrial practice are the ball mill, the autogenous (AG) and the semi-autogenous (SAG) mill. Tumbling equipment is further categorised by the mechanism of size reduction. A ball mill is composed of a hollow shell partially filled with balls, at approximately 40% volume fraction, and a given material charge. The balls are usually made of various grades of steel, iron or ceramic, depending on the size of the mill and the properties of the material being milled. The inside of the mill is lined with lifters, to raise and propel the charge, and replaceable liners, to extend mill duration. These are usually made of wear resistant steels or rubbers.

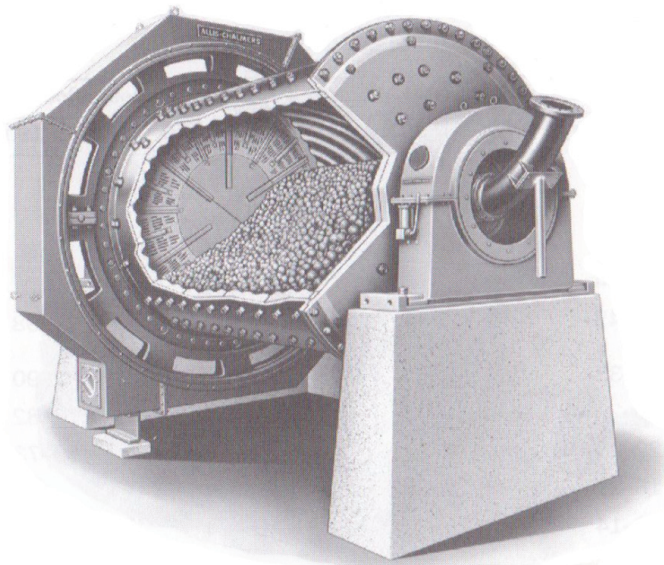


Figure 2-2: Ball Mill [1]

When the mill is rotated, the mill charge will begin tumbling, whence the generic name for these mills, tumbling mills. The motion of the balls in the mill will result in comminution events, when particles are caught between tumbling balls, or between the balls and mill liners, and crushed or ground down. A semi-autogenous mill, or SAG mill, is similar to a ball mill, though much larger. It uses a smaller amount of larger balls than the ball mill and the ore charge is generally of a much larger particle size. In these mills, comminution occurs due to impact of the particles with each other and with the falling balls. The autogenous mill, or AG mill, uses the same principle, but exclusively relies on inter-particle impact. AG and SAG mills serve primarily in the range of secondary crushing to coarse grinding, as seen in Table 2-1, and are usually upstream from ball mills, which range from coarse grinding down. Other mills, similar in principle, are rod mills

and stirred mills, which are usually in finer applications, such as ultrafine grinding or regrinding.

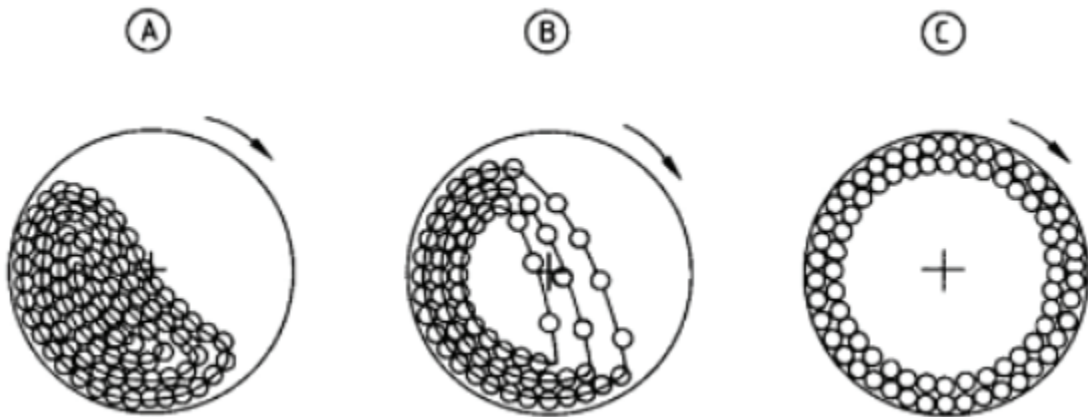


Figure 2-3: Mill charge motion: (a) cascading, (b) falling, (c) centrifugal [2]

The only components constraining the contents of the mill charge inside the mill are the mill shell and the other elements of the charge. When the mill is rotated, the charge will adopt a certain profile, as shown in Figure 2-3. At low speeds, the charge begins cascading, where balls run down over the charge from the top, or head, to the bottom, or toe, of the charge. In the falling phase, balls are projected from the head into the air inside the mill and fall on the toe, or on the mill liner. If the mill is rotated at a sufficiently high speed, the charge will be trapped along the inside of the mill, i.e. will centrifuge [2]. The charge profile of a given mill will be determined by various parameters used in the mill design. The friction generated between the individual elements of the mill charge, and between the charge and the mill wall, the shape of the mill wall liners, and the profile given to risers in the walls, will determine how balls are carried in the charge [8]. By altering the charge motion profile, the nature and intensity of the interactions occurring in the mill charge can be controlled [1, 8-10].

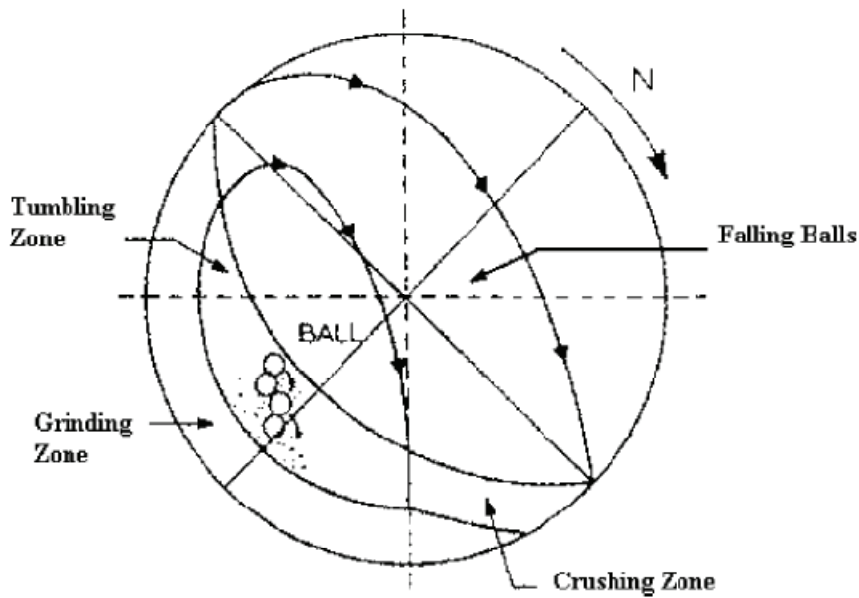


Figure 2-4: Mill charge profile [11]

The profile of the mill charge depends on the motion of the charge elements and the rotational speed of the mill, resulting in three distinct zones: the tumbling, grinding and crushing zones, differentiated by the particle breakage mechanism occurring [11]. The crushing zone is characterised by ore particles caught in high-energy impacts from balls thrown from the head of the charge to the toe. In the tumbling zone, the balls rolling over each other, crushing ore in low-energy impacts. The grinding zone is characterised by balls sliding and rolling against each other, breaking by abrasion the particles caught between the balls [11, 12]. Cascading charge motion leads to tumbling and grinding, while falling motion results in falling and tumbling. Centrifugal charge motion rarely occurs, as it is generally not productive.

The principle of using the tumbling motion of a charge to generate mechanical action on particles is not only in mineral processing, but in other,

more exotic fields. Ceramic processing, for example, uses ball mills to generate a powder feed material for ceramic fabrication [13]. In the field of nanoengineering, stirred mills are used to create nanostructured materials, for use in various applications. Metallic powders are loaded into mills cooled with liquid nitrogen, and charged with small steel balls, which are stirred. The small metal elements are then mechanically compressed when caught between two surfaces, as is the case in the ball mill. Due to the ductility of the metal powder particles, they are alternatively deformed and worked together, with a sufficiently long work period, this eventually leads to the formation of nanostructured powders [14, 15]. In these applications, iron contamination from grinding media wear is a serious issue, usually avoided by replacing steel grinding media with something containing a composition close to the material being milled.

The configuration, design and size of a comminution device will be determined by its position and purpose within a mineral processing system, as well as the mineral being handled and available capital for equipment purchasing. Large, primary crushers will be found at the front of the processing stream, to handle the sizable material being fed in at high tonnages. Travelling along, as the material becomes increasingly finer; other pieces of equipment will be employed, as per Table 2-1. In the plant circuit, comminution equipment will be alternated with various pieces of classifying equipment, used to select between different material sizes. After a comminution device, the discharged material will be classified. Material which is sufficiently fine will be directed onto further stages of processing, while material insufficiently reduced will be returned to the

previous stage [4]. In this manner, through the use of a recirculating load, material may be processed more thoroughly and completely. The comminution equipment used will be decided based on the tonnage to be processed, the geological properties of the material, and the performance parameters of the equipment.

With regards to the design of a ball mill, only generalities may be discussed, due to the complexity of mill design, and the wide variations in use environment [3]. Ball mills are designed using design guidelines, as well as empirical sizing equations which equate mill dimensions with tonnage throughput [3, 16]. Similarly, equations have been developed to determine the mill charge volume, both in terms of media and in terms of rock. Grinding media charge size can be calculated based on the abrasivity of the ore, the size of the rock feed and other known correlation factors [16]. Mill running speed can be determined based on empirical relationships, as well as through computer charge modelling. An element of importance in milling is the use of water. Ore may be milled wet or dry, depending upon end use and processing conditions. Most material is milled wet, due to the position of the mill in a processing stream, where the feed may come from an aqueous process, or the product is to be sent to another type of aqueous processing. In dry grinding, for fine product sizes, some degree of cushioning occurs at interfaces, reducing the amount of wear occurring in the system, but also reducing the energy efficiency of said system. In wet grinding, size reduction is much more efficient, with a finer product size generated, at the cost of increased wear [17]. This system is also advantageous in terms of reduced

dust control requirements, reduced power consumption and easier integration into classifying systems[17].

2.1.4 Comminution models

Beyond simple understanding of the comminution process, techniques are required to measure, quantify and compare comminution events for different pieces of equipment and different ores. Early attempts by Kittinger and Kick tried to link particle size and comminution work [4]. Bond studied these attempts and, through experimental work, developed what is now known as the Bond Work Index. This formula is known in many forms, but can be simplified as

$$W = W_i \left(\frac{1}{\sqrt{F_{80}}} - \frac{1}{\sqrt{P_{80}}} \right) \quad \text{Eqn. 1}$$

where W_i is the Bond Work Index, F_{80} is the particle size in microns through which 80% of the feed should pass and P_{80} is the size through which 80% of the product should pass [1, 4]. This formula is the result of empirical testing, and is a compromise between the theories of Rittinger and Kick [4]. It has become, over the years, the standard in quantitative measurements of multi-particle comminution, and Bond Work Indices for various materials are widely measured and known [4, 16-19].

While the accepted standard in evaluating ore particle breakdown due to comminution, the Bond Work Index does have a few limitations. The value of the work index W_i given in the literature for a given material refers to a theoretical size reduction from infinite size to 80% passing 100 μm , occurring in an eight foot

diameter ball mill using closed-circuit wet grinding [1, 18]. It has been used far beyond its original intended purpose [20].

Another means of quantifying comminution is the JK Drop Weight test, which generates a Drop Weight index, DW_i [18]. This technique places ore samples of a single size class into an impact tester, onto which a weight is dropped to induce breakage. This test is repeated for different size classes and force ranges to generate a t_{10} graph, where t_{10} designates the fraction of particles finer than one-tenth the original size class, whence why the Drop Weight index test is often referred to as the t_{10} test. Results are plotted and fitted using

$$t_{10} = A(1 - e^{-b \times E_{CS}}) \quad \text{Eqn. 2}$$

where A and b are curve fitting parameters and E_{CS} is known as the specific comminution energy [18, 21]. It is the term used to describe the energy per ton of ore needed to induce comminution in impact breakage. This holds interesting properties for comminution measurement and modeling.

2.2 Wear

2.2.1 Introduction

Wear is defined as a mass-loss process occurring at the surface of a material when subjected to forces caused by interactions of the surface with another element or surface, resulting in the displacement or removal of the surface material [22, 23]. Wear is caused by a variety of potential mechanisms, as determined by the nature of the interacting surfaces, and the means through which they interact. There exists some disagreement on the amount of individual wear

processes, and whether certain mechanisms can be classified as wear, or how they can be grouped, divided and subdivided [22-25]. For the purpose of this work, four major mechanisms in wear are adhesion, fatigue, erosion and abrasion. In discussions of wear, the term *system* is used to denote the context in which wear occurs. This describes the total set of conditions occurring during the wear incident, such as the nature of the surface worn, the nature, magnitude and direction of the forces causing wear and the environmental parameters that influence the wear response.

2.2.2 Adhesion, fatigue and erosion

Adhesion and fatigue are two of the four mechanisms by which wear occurs in interacting surfaces. Adhesion is caused when two flat material surfaces are in sliding contact with each other [22]. Due to the nature of small scale surfaces, even technically smooth surfaces are rarely perfectly flat. Surfaces, no matter how smooth, will have a certain number of asperities. When two surfaces are in contact, while the nominal contact area may be quite large, the actual contact area is limited to the contacts between the asperities of the two surfaces, which is a much smaller area [22]. An example of two interacting surfaces is seen in Figure 2-5.

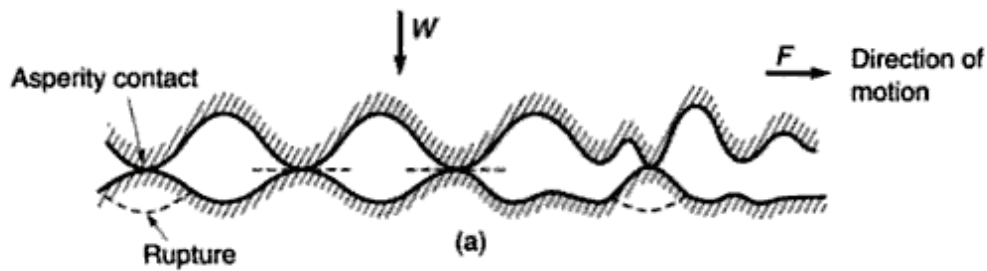


Figure 2-5: Adhesive surface interaction [22]

For a given applied force, the actual pressure experienced at the contacts will be higher than the nominal pressure. The pressure experienced may be sufficient to induce plastic deformation in the contacts between the surfaces. The outermost atoms in the interacting surfaces will be quite close to each other, particularly in situations where both surfaces are clean and uncontaminated [23]. This can lead to the formation of adhesive bonds between the surfaces, which may be quite hard to break. The bond at the surface junctions may be of the same order of strength as the bulk strengths of the two interacting materials. Separating the surfaces requires the application of a large normal or shear force. Due to the strong nature of the bond, particularly in ductile metals, the force required to separate an adhesive interface may be greater than the forces required to shear the asperities themselves from the surface on which they are present [23]. This leads to wear, through the localized shearing of surface asperities from the surface of the sample. In comminution equipment, however, adhesive wear is not a major concern. For adhesive wear to occur, adhesive bonds need to be formed between interacting surfaces in sliding contact. The adhesive strength of an interface is determined by the composition of the two interacting surfaces, as well as their respective

topology [22]. Adhesion is highest between two interacting surfaces with identical composition, in a perfectly clean interface with a low surface roughness [23]. The presence of any foreign surface contaminants, oxide films or foreign bodies between the two surfaces will disrupt the adhesive force quite effectively, by preventing any adhesive bond from occurring [22]. Liquids present at the interface will reduce the shear strength required to move the two surfaces relative to each other, reducing friction coefficients [22]. Mineral processing systems are full of contaminants, foreign bodies and liquids at potential adhesive interfaces, dramatically lowering the influence of adhesive wear.

Fatigue wear is caused by the repeated application of mechanical loads against a given surface, leading to long, cyclical periods of stress and strain. This usually occurs in conditions of rolling or sliding contact [22]. While the applied forces are not enough to directly induce wear themselves, they create low levels of stress in the material. This repeated, long term strain will eventually result in the formation of cracks in both the surface and bulk of the stressed material [24]. After sufficient cycles, these cracks will grow to a point where the material fails. This failure, which is often catastrophic in nature, results in the generation of wear fragments at a location where little or no wear was seen previously [24]. With regards to mineral processing equipment, fatigue may be a concern for some types of fixed equipment, as with all mechanical systems. However, for the comminution mill *charge*, fatigue is a smaller problem due to the limited duration of this material. In a great deal of these applications, fatigue is not an issue, as by the time fatigue wear becomes a problem, other, more aggressive processes will

already have been at work for a long period of time, having already damaged or destroyed the material. It can be seen in impact related damage, where material losses are low over time, but deformation can be quite significant. This, in part, is why mills have mobile charges that are replaced as depleted, and liners are replaced after a certain lifetime. It is significantly less expensive to replace a mill's lining, than the mill itself [17].

Erosion is the wear process that occurs when small particles, carried in a fluid, strike the surface of a given material, inducing damage [24]. Tribologically, erosion is differentiated from abrasion in that the abrasive particles are carried by a fluid and impacted against the surface of the material, instead of sliding or being dragged along the surface [22]. Several factors will influence the erosion experienced by a surface. The amount of erosive particles, as well as their hardness and shape, will alter their effectiveness. The nature of the carrying fluid, whether gas or solid, as well as its velocity, will determine the energy imparted by a given particle impact. The nature, hardness and temperature of the impacted surface will also be of importance. One important parameter is the impingement angle, which is the angle at which the erosive particles strike the surface. In ductile materials, the highest wear occurs at shallow angles, where the erosive agent strikes a glancing blow against the surface, which results in shearing of the surface [24]. In brittle materials, such as ceramics, an erosive agent induces more wear with an acute impingement angle, where the incoming particle strikes the surface dead on, resulting in fracture in the material [24]. Erosion can also be caused in strictly fluid systems, in cases with very high fluid velocities. If the

drops of a liquid are directed against a surface with very high speeds, these can also cause erosion, due to their high kinetic energy, which leads to high pressures on impact. Cavitation, which is the creation of a short lived gas bubble inside a fast-traveling fluid when the pressure inside a fluid falls below the vapour pressure, may also contribute to erosion. The existence of the bubble, and its rapid collapse, creates a shock wave in the fluid that can damage the surface of the material. Erosion is a serious concern in mineral processing systems, where large amounts of erosive particles are carried through countless pipes, reaction vessels, tanks and many other pieces of equipment. Erosion, however, is not a primary concern in comminution equipment, once again due to the fact that other processes occurring in that equipment are much more aggressive.

2.2.3 Abrasion

2.2.3.1 Introduction

Abrasion is one of the processes responsible for wear. It is caused by the motion against a surface of an abrasive agent, either another surface or abrasive particles. This motion, coupled with the pressure created by the resultant force over a localized region of the surface, will lead to localized stresses in the surface, resulting in plastic deformation at the interfaces.

2.2.3.2 Abrasion mechanisms

The action of the abrasive agent against the surface depends on the nature of the surface, the agent, and the pressure at which they are brought together. This will result in different wear behaviour, as shown in Figure 2-6 [25].

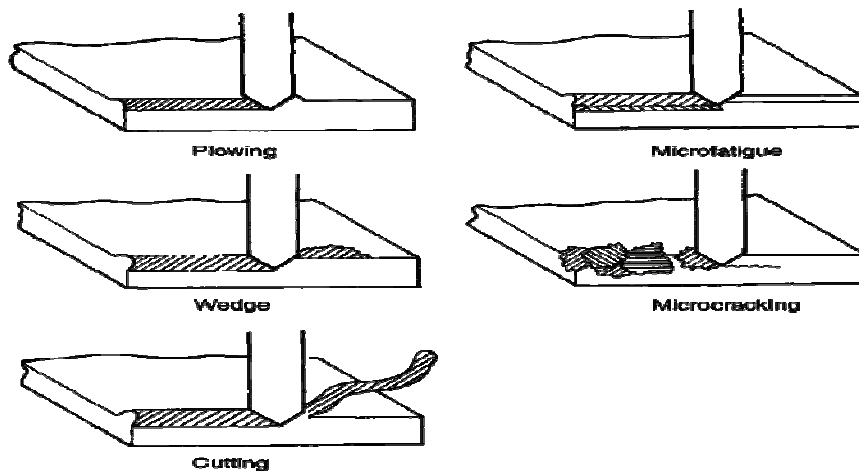


Figure 2-6: Abrasive wear mechanisms [25]

In this figure, the five abrasion mechanisms can be seen in a simplified view. These mechanisms are ploughing, wedge formation, cutting, microfatigue and microcracking. Ploughing occurs when the abrasive agent displaces material from the wear track to the side of the track [25]. An example can be seen in Figure 2-7, from the work by Hokkirigawa and Kato, who studied abrasive wear using a steel pin against various metal surfaces [26].

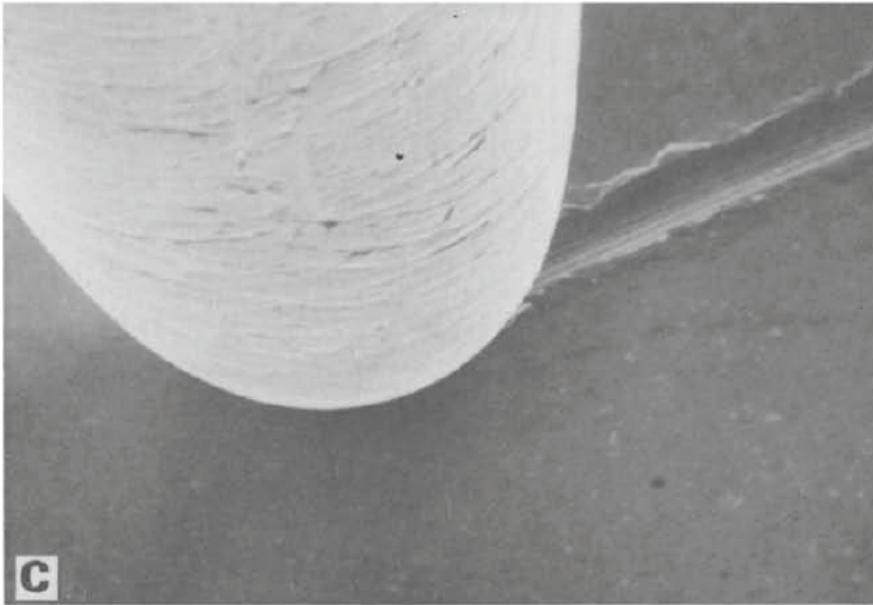


Figure 2-7: Ploughing, steel pin against brass [26]

The material is not removed from the surface, but is simply displaced to the side, while a groove is formed in the surface [22]. The second mechanism is wedge formation. In this process, a certain amount of material is displaced from the wear track, and accumulates in front of the abrasive agent [25]. Figure 2-8 offers an example, once again from Hokkirigawa and Kato, of wedge formation in an abrasive interface [26].

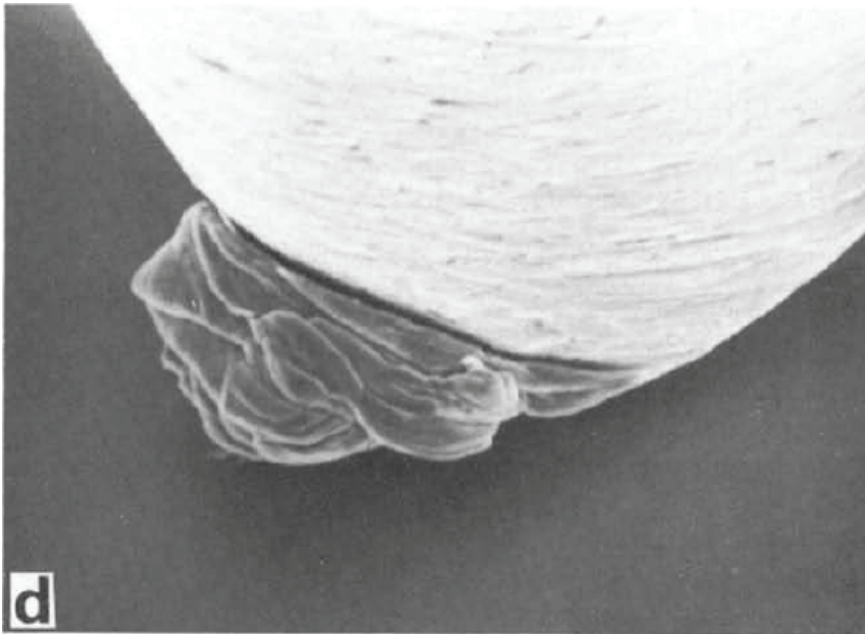


Figure 2-8: Wedge formation, steel pin against stainless steel [26]

In this case, the material has been plastically deformed and displaced from the surface to accumulate in front of the abrasive agent. The third mechanism is cutting, in which the abrasive cuts out a portion of the surface, displacing it out [25].

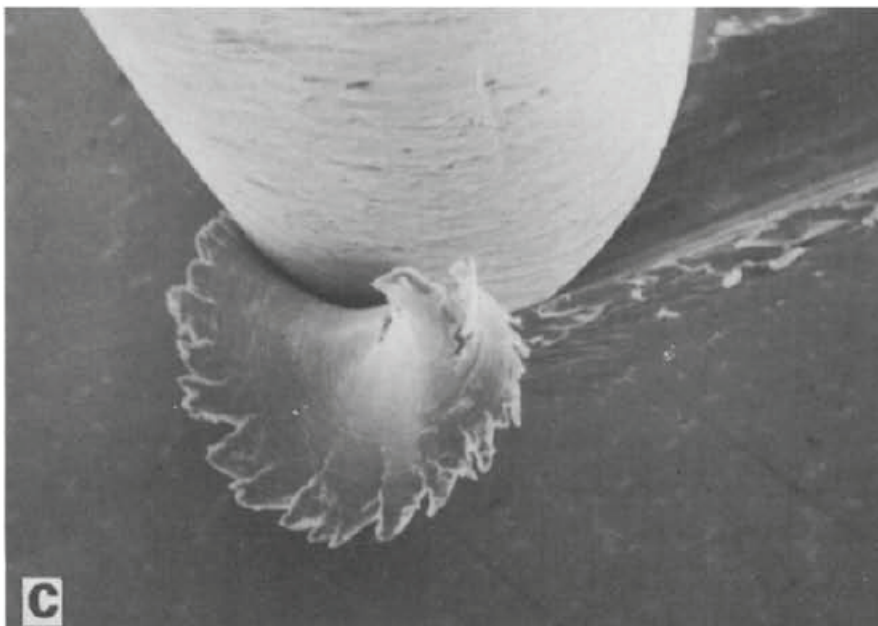


Figure 2-9: Cutting, steel pin on brass [26]

In cutting, as seen in Figure 2-9, the material is wholly removed from the surface as a ribbon of cut material, with little or no displacement to the side. This constitutes the most aggressive form of wear occurring in ductile materials [25]. While all three of these mechanisms can and will occur in an abrasive system, the dominance of one over the other two will be determined by such factors as the attack angle of the abrasive agent, the degree of penetration and the shear strength of the interface [22]. With a sharp abrasive tip, there is a critical angle that separates cutting from wedge formation and ploughing, depending on the material. The degree of penetration determines the balance between ploughing and wedge formation to cutting, due to an increase in the coefficient of friction with greater penetration. The interfacial shear strength determines the balance between ploughing and wedge formation. In systems where the ratio of interfacial shear strength to bulk strength is high, only a portion of the material will be displaced to the side, while some will accumulate in front of the abrading agent [22].

Microfatigue occurs in systems where an abrasive agent passes over a wear track repeatedly, inducing localized stresses, even in systems where little or no direct wear occurs. This induces fatigue in the materials, which will eventually fail. Furthermore, when an abrasive agent displaces material in ploughing and wedge formation, it induces localized strain hardening in the displaced material, resulting in a degree of cold working. Further passes over the displaced material generated by previous wear events will result in more fatigue, eventually leading to failure [25]. Microcracking occurs primarily in brittle materials, such as

ceramics. In this case, the abrasive agent is applying sufficient pressure to the brittle material to induce fracture in the surface grains.

2.2.3.3 Abrasive system configuration

Another element of importance in an abrasive system is the manner in which the abrasive event occurs, as determined by the nature of the interfacial interaction. In any abrasive system, there exists a surface of interest, hereafter referred to as the primary surface, against which a force acts to induce damage. This force is applied by, another surface, hereafter called the counter-surface, or abrasive particles. While one surface is being specified as the one studied, due to the interest invested in that surface, in all reality, both surfaces are experiencing friction, which induces wear. It is simply that one surface may be of more interest in a given experimental system investigation[25]. This is illustrated below in Figure 2-10, where the bottom surface in each pair is the primary surface, or the one of interest in that system.

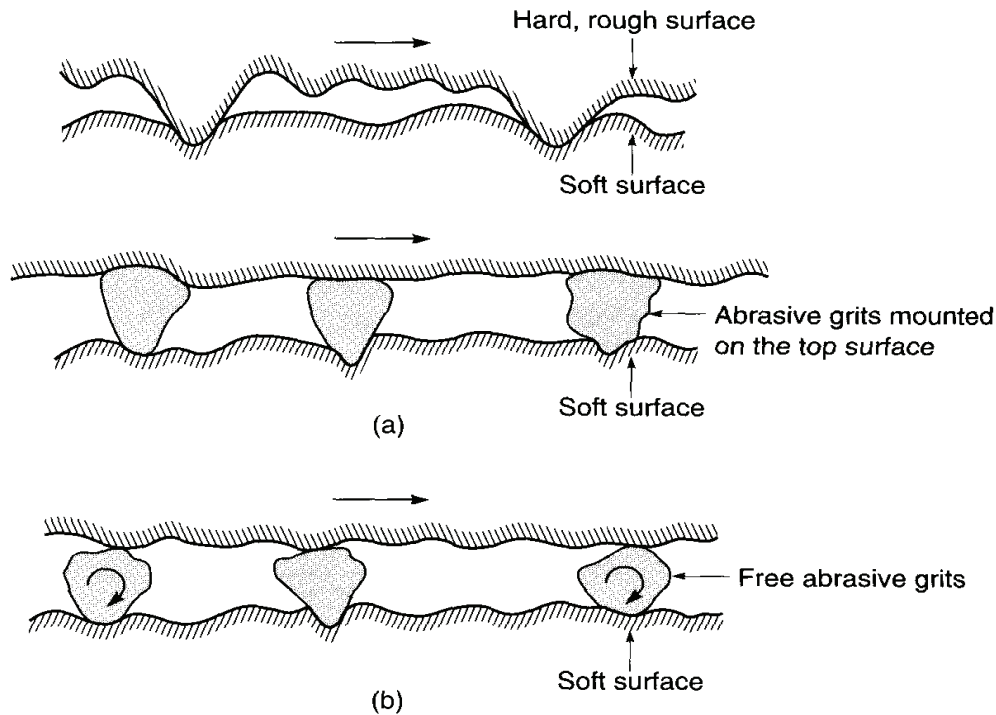


Figure 2-10: Abrasive system configuration [22]

This figure illustrates the three major configurations possible in an abrasive system. The first is composed of two interacting surfaces, where the asperities of one hard, rough counter-surface are used to abrade the surface of the softer primary surface. The second case shows the situation where abrasive grits are attached to the counter-surface, which carries them in their abrasion of the primary surface. In this system, the abrasive agents have their motion restricted by their attachment. A common example to illustrate this case is sandpaper, where abrasive grits are glued to the surface of the paper and are used to abrade a surface to make it smooth. The final image illustrates free abrasive grains caught between two moving surfaces [22]. In all of these systems, abrasion is caused by the relative motion of one body against the other or others.

This highlights a distinction made in abrasive systems, between two-body and three-body wear, in open and closed systems [27].

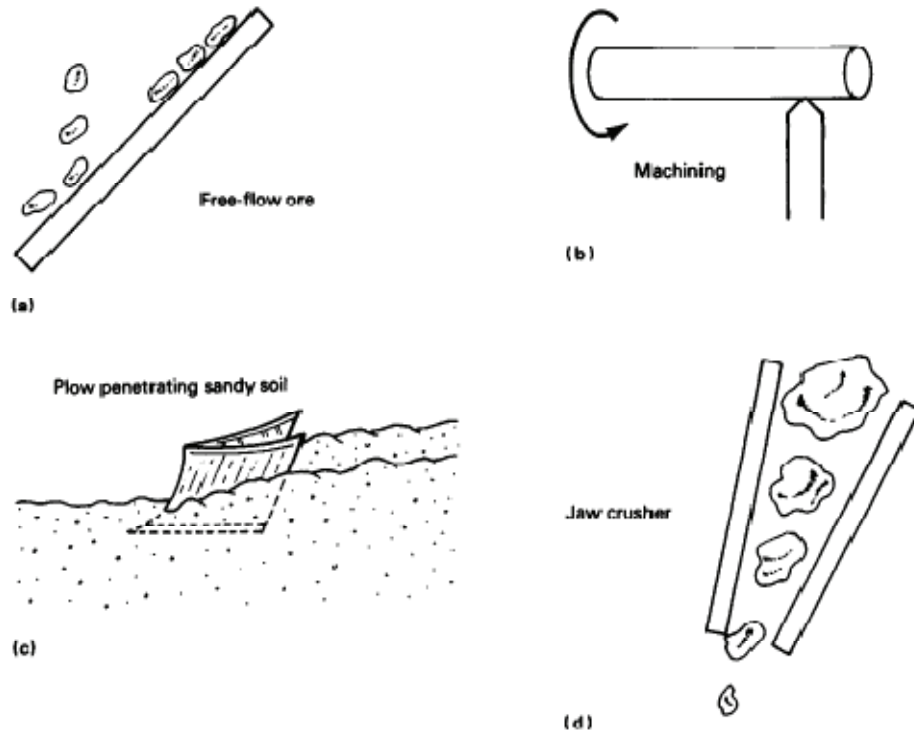


Figure 2-11: Abrasive system configuration, (a) open two-body, (b) closed two-body, (c) open three-body, (d) closed three-body [25]

According to Misra and Finnie, open wear is defined as occurring when the wear occurs on only one surface, or the two surfaces are far apart, while closed wear occurs when abrasive particles are constrained in position [27]. Meanwhile, two-body abrasive wear occurs when an abrasive agent slides along a given material surface, while three body abrasive wear requires the action of three, or more, bodies in a given systems, where one body, the particle, is constrained between two surfaces [27, 28]. Open two-body wear would be familiar to any processing engineer knowledgeable in materials handling systems such as

discharge chutes or on screen decks, where loose abrasive material runs over an exposed surface. Closed three-body wear dominates in comminution applications, where an abrasive agent is constrained between two surfaces, either comminution media, mill liners or crusher wear surfaces.

Abrasion processes are further defined as being either low-stress or high-stress. Low abrasion events described as low-stress occur when little or no damage occurs to the abrasive material. High-stress wear, meanwhile, describes situations where the abrasive material is crushed during the abrasion incident [12, 25, 27, 29]. In this case, the forces at the abrasion interface are such that the fracture strength of the abrasive particle itself is exceeded, leading to particle fracture [29]. Other mechanisms are sometimes suggested for abrasion. Gouging is used to describe systems where an abrading agent removes a significant amount of surface material in one abrasion incident [25, 27]. Polishing wear describes a state where very small interactions with small abrasives generate a smooth, shiny surface [25]. From a comminution standpoint, high-stress wear is prevalent in interactions occurring between media in a mill, as the goal of these mills is size reduction of the abrasive agents. It is desired to have the equipment running in high-stress wear, as this results in particle fracture, which is the purpose of comminution. This evidently has ominous implications for comminution media wear. Gouging is often seen in equipment such as those described in Table 2-1 as primary or secondary crushers. A perfect example is a jaw crusher, as described previously and shown in Figure 2-11, which handles sizeable rocks and suffers primarily gouging wear.

2.2.3.4 Hardness

One of the key parameters in the wear experienced by surfaces in abrasive systems is the hardness of the respective surfaces and abrasive agents, as well as the relative ratio between the hardness of these different elements. In general terms, for both two and three-body abrasion, wear resistance in a surface material increases with increasing hardness [24, 25, 30]. In the case of three-body wear, the hardness of the abrasive particles also has an influence, or, more properly, the ratio of the hardness of the abrasive agent to the surface hardness [24]. Wear on the surface is highest when the abrasive material is harder than the surface, and lowest when the abrasive is softer than the surface. Hard abrasives lead to high abrasion, while very soft abrasives lead to little or no abrasion [31]. This is illustrated in Figure 2-12.

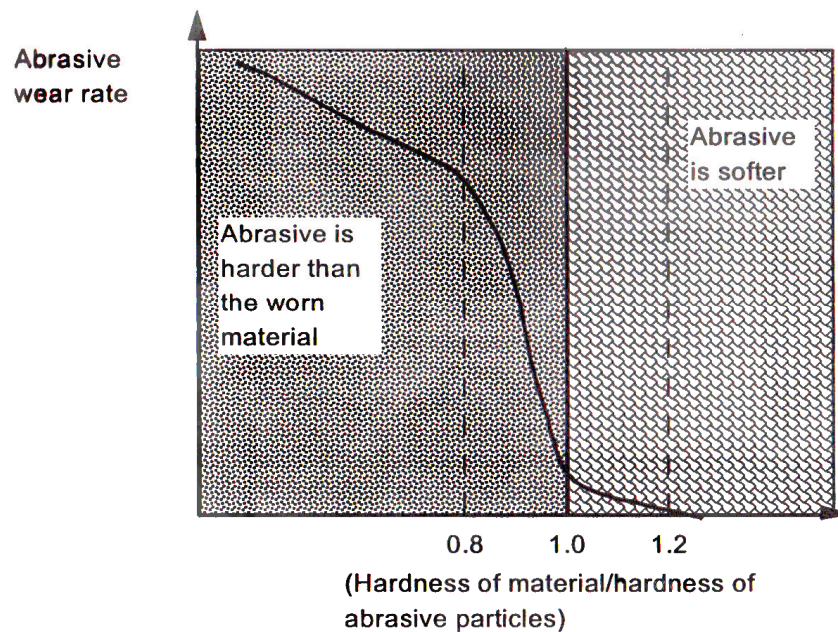


Figure 2-12: Wear rate as determined by relative hardness ratio between surface and abrasive agent [24]

The ratio of hardness between the interacting surfaces is important. In two-body abrasion, when one surface is much harder than the other, this surface will act as the abrasive agent, while the other will be abraded and incur most of the wear. In three-body wear, the relation between the primary surface and counter-surface will determine the motion of the abrasive agent. If one surface is significantly softer than the other, then the abrasive agent will be imbedded into the softer material, and will be dragged along the surface of the harder material, resulting in a sliding motion for the abrasive. If the two surfaces have similar relative hardness, the abrasive agent will roll between the two surfaces, instead of sliding along [30]. One of the most common and recommended means of reducing the wear experienced by a given surface is to make it harder than the other surfaces with which it interacts [22, 24, 31, 32]. Care must be taken, so that the surface is not so hard as to crack and fracture due to applied forces [22]. Furthermore, this may result in increased wear against the counter-surface. In most circumstances, this requires careful engineering design. It may be preferable, from maintenance and cost perspectives, to adjust the relative hardness of interacting surfaces so that one component, more easily and cheaply replaced, experiences the brunt of the wear, sacrificed to lower the wear on more complex or expensive components. This is often seen in gear assemblies, where some will be made of hard steel, while others will be of brass. The softer brass gears will experience the majority of the wear, while little or no wear will occur on the steel gears. The system is then designed so that the brass gear can be easily and cheaply replaced, facilitating maintenance and reducing overall costs.

2.2.3.5 *Abrasive morphology*

The size and shape of the abrasive particle have an influence on the wear rate of a material. Angular particles, with sharp edges, are known to be more abrasive than rounded particles [33, 34]. These particles have been shown to be more effective in causing wear in low-stress abrasion. Interestingly, in high-stress abrasion, it has been found that the fractured particles generated in the abrasion event are among the most effective materials for abrasion [29, 33, 34]. Freshly fractured particles are particularly effective at abrasion, as the fresh abrasive surfaces are generated and encounter the wear surface near instantaneously in-situ. This has an interesting implication for the difference between low-stress and high-stress wear. It was seen by Dube and Hutchings that while particle abrasivity was influential in low-stress abrasive wear, it had little effect in high-stress wear [34]. No matter the initial shape or angularity of the material, high-stress wear lead to the fracture of the abrasive grains, resulting in fresh abrasive material. While there was a sizable difference in wear rates between particles of different angularity at low-stress, little difference was seen in high-stress abrasion situations [34].

The size of the particle will also have an effect on the wear rate. It has been seen that in most cases, larger particles will induce a higher wear rate than particles with an identical composition but smaller size [34, 35]. This hold true to certain sizes, after which size becomes less important [29]. Things become more complex in the case of metal matrix composites, when using abrasive agents smaller than the reinforcement phase. In this case, the small abrasive elements can

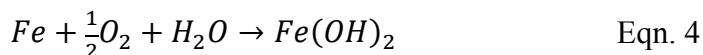
wear away at the matrix without touching the reinforcement at all, until the matrix is worn away and the reinforcements fall out. In this situation, smaller particles, capable of interaction with only the matrix while bypassing the reinforcement phase, will induce higher wear rates [36].

2.2.4 Corrosion

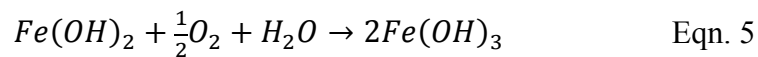
Corrosion is defined as a mass loss process where the surface of a material deteriorates as a result of dissolutive environmental reactions [13]. It is an electrochemical process where metal atoms present in a solid lose electrons and are released as ions into a solution, according to the generic reaction below,



where a metal releases n valence electrons, acquiring a charge of $+n$. These electrons will react with various other ions in solution, to complete the electrochemical couple. Iron, the primary element in steel comminution media, will corrode in water, to form rust, according to the reactions



and



For corrosion to occur, a few conditions must be met. A favourable electrochemical potential reaction must exist in the system, which requires the existence of an electrochemical couple. For iron, oxygen is effective. Furthermore, the reaction requires a sufficiently conductive medium for electron motion to occur. Water containing various salts and impurities will be sufficient. Corrosion will be affected by environmental parameters in the mill, such as fluid velocity,

temperature and composition. High fluid velocities will result in increased corrosion, due to increased agitation. High temperature promotes corrosion, due to improved reaction kinetics [13]. A piece of comminution equipment like a ball mill is, for all intents and purposes, the worse possible conditions imaginable with regards to corrosion resistance. It contains large amounts of steel, in an agitated slurry composed of water and various metal-rich minerals, forming an aqueous soup of ions well supplied with oxygen and at high temperatures.

Corrosion can be minimized through various means. The first and most obvious is to remove the galvanic couple by removing the oxidizable surface from its corrosive environment. The environment itself may also be modified to reduce the concentration of reactive elements. In cases where these mitigation techniques are not feasible, proper material selection should be employed to select for corrosion resistance. One possibility is to select an inert material, which will not react in the corrosive environment at all. In other cases, some materials, such as stainless steel, possess a passivation layer which increases their corrosion resistance by acting as a physical barrier to the electrochemical couple. This, however, may not always be effective. In abrasive or erosive systems, the protective passivation layer may be disrupted or removed by mechanical effects of abrasion or erosion. This will accelerate the degradation of the surface due to synergistic effects between the corrosion and abrasion, leading to a higher overall mass loss rate [13, 24].

2.3 Abrasion modeling and measurement

2.3.1 Introduction

From an understanding of the mechanisms involved in wear, it may be possible to model wear in a real system. One of the earliest models by Rabinowicz simplifies abrasion to a cone penetrating a surface and moving through that surface, as shown in Figure 2-13.

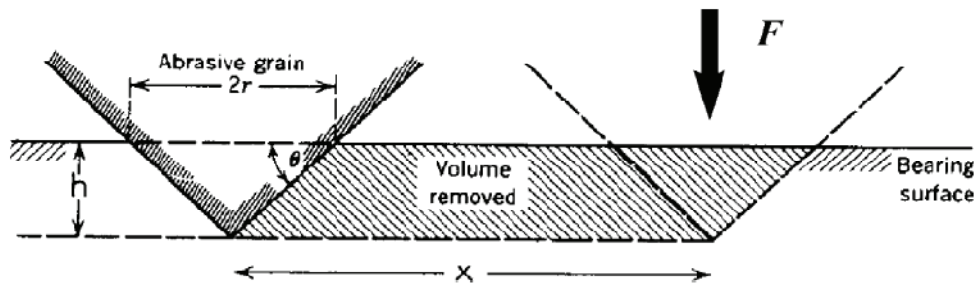


Figure 2-13: Rabinowicz's abrasive wear model [37]

In this model, the application of a force F to the cone leads to penetration into the material of hardness H to a depth of h [37, 38]. When the abrasive cone is moved a distance x , it removes material from the surface according to the formula

$$V = \frac{Fx(\tan\theta)}{\pi H} \quad \text{Eqn. 6}$$

If the term K is substituted for $(\tan\theta)/\pi$, this gives the equation

$$V = K \frac{Fx}{H} \quad \text{Eqn. 7}$$

where K is a dimensionless abrasion constant.

This is quite similar to Archard's wear relation, where the wear w is directly proportional to the load on the surface W and inversely proportional to the surface hardness H , such that wear can be described as

$$w = K \times \frac{W}{H} \quad \text{Eqn. 8}$$

where K is a dimensionless abrasion constant known as the wear coefficient [23]. Both of these relations are technically similar, and may be expanded to describe the mass lost during an abrasive wear event as a function of force and material density, according to an expanded Archard relation

$$m_a = \rho \frac{\tan(\theta)}{\pi H_r} Nx \quad \text{Eqn. 9}$$

where m_a is the mass abraded, ρ is the density, θ is the abrasion grain angle, H_r is the hardness, N is the applied normal load and x is the distance of travel[39]. Abrasion can then be measured and quantified in systems where an abrasive agent acts along a surface.

This relation is one of the principles behind several tests used to quantify wear of abrasive materials on a given surface. Several standards have been developed to measure wear rates. A great number of tests use a pin-like object and a surface to which abrasive grains were bonded, such as ASTM G132-96 Pin Abrasion Testing [40]. While commonly used for tribological systems, this technique has several problems for use in comminution testing [35, 41, 42]. As the abrasive material is bonded to the sheet, it is not free to move or roll, but is locked in a sliding position, with a subsequent effect on the wear mechanism. Additionally, depending on the system design, the pin may pass over a given surface repeatedly, such that it does not always encounter fresh abrasive grains, reducing the amount of wear occurring. This type of test is therefore limited in its applicability to comminution systems [12].

2.3.2 Rubber Wheel Abrasion Test

Another very common technique that is widely used to simulate three-body wear is ASTM G65: Dry Sand/Rubber Wheel (DSRW) test, which is a test designed to measure the abrasion resistance of given material surfaces. In this test, a flow of abrasive material is directed between a sample and a rubber-lined steel wheel, which is then pressed against the sample and spun with a given rotational speed. The rubber then pulls the abrasive material down between the wheel and the sample, forcing the abrasive against the sample and creating a scratch, resulting in this test's other name of Rubber Wheel Abrasion Test (RWAT).

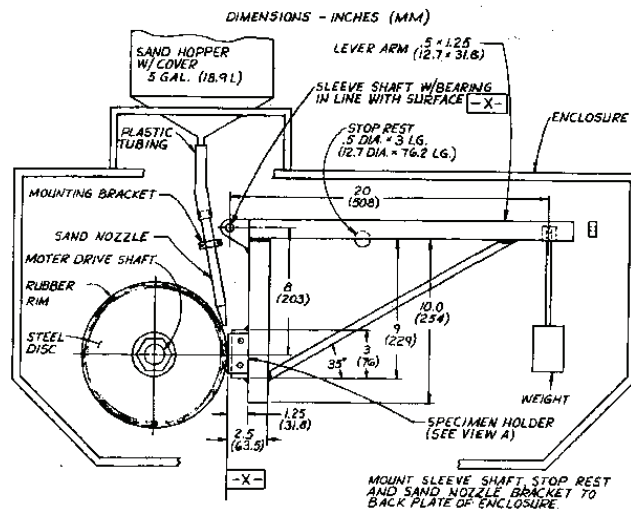


Figure 2-14: ASTM G65 Dry Sand Rubber Wheel test[43]

Wear is measured as the mass or volume lost during a test, for a given set of abrasion conditions. This test is widely seen in the literature to measure three-body abrasion in a given tribological system [12, 27, 29, 33, 34, 36, 44-46]. The standard specifies a sized silica foundry sand at a given flow rate, with

standard values for runtime, applied force and system settings. Variations are also used to measure wear caused by wet sand or slurries [47]. The DSRW test has been shown to operate in low stress, three-body wear, as abrasive agent breakage is quite small [8, 12]. This poses a problem in studying wear during comminution, due to insufficient particle breakage.

2.3.3 Ball Mill Abrasion Test

Another approach to measuring three-body wear in tumbling mills is to actually carry out the test *in* a laboratory ball mill, which is known as the Ball Mill Abrasion Test (BMAT). A mill is loaded with the comminution media, abrasive materials, liquids and gasses of interest for a system and run to carry out the experiment as close to system parameters as possible. Degradation on the comminution media is measured by marking and measuring the element of interest before the test, and measuring the degradation experienced as mass loss for the same elements after the test. Breakage of the abrasive can be quantified by sizing the feed material before and after the test, comparing the two values. Advantages of this type of test are that it replicates the conditions occurring in an industrial mill, with abrasion, impact and corrosion occurring simultaneously. Conditions can be adjusted to simulate, to a certain degree, the conditions in a given system [12, 48-51]. Using a laboratory-scale ball mill, however, has certain problems for comminution measurements. While the test does replicate the nature of the motion inside a commercial mill, the forces involved are not necessarily the same, due to effect of scale. Laboratory mills will have a diameter on the order of less than half a meter with a few kilos of mill charge, while real mills will have

diameters of several meters, and several tons of mill charge. The forces occurring in the mill do not all scale linearly with mill size, such that effects occurring in the laboratory may not be adequately be represented in the field, and vice versa. Corrosion, for example, has been shown to account for between 25% to 75% of material loss in laboratory mills, while only accounting for approximately 10% of material loss in industrial trials [50]. The test replicates the motion of the test, but not necessary of the material flow. In most operations, mills are fed continuously, while laboratory test operates as a batch process, which means that broken abrasives are not ejected and replaced in the BMAT. Furthermore, this test requires a great deal of ore and media for a single test, making any test work cumbersome, time consuming and potentially expensive. While degradation caused by abrasion, impact and corrosion can be measured together in this test, it is also difficult to determine the contribution provided by each component.

2.3.4 Steel Wheel Abrasion Test

The Steel Wheel Abrasion Test (SWAT) is an attempt to employ the test principles behind the RWAT as described in ASTM G65, an effective test replicating low-stress three-body wear, while generating sufficient breakage to enter high-stress three-body wear. In this system, the rubber-lined steel wheel used to apply a force to the abrasive and slide it along the sample surface is replaced with a full steel wheel. The experimental process and the equipment remain fundamentally identical; indeed an ASTM G65 compliant RWAT machine can be converted to a SWAT rig by replacing the test wheel. The resulting abrasion event, however, is altered. The steel wheel, being inherently significantly

less compliant than rubber, will induce greater pressure in the abrasives, promoting greater breakage and the shift into three-body wear. Furthermore, the steel wheel is capable of exerting significantly higher forces on the sample. While ASTM G65 specifies that the applied force on the sample should not exceed 150 N, due to machine limitations arising from the use of a rubber layer, the SWAT can exert forces of up to 1000 N onto the sample [8, 39, 43]. These higher forces permit abrasion tests to be carried out in force ranges similar to those occurring during the interactions between different elements of tumbling mill charge elements. The steel wheel abrasion test has been used to replicate high-stress three-body abrasive wear in an controlled test [8, 28, 33, 39]. Ironically enough, the RWAT described in ASTM G65 can trace its development back to wear measurement apparatus developed by Brinell, which used an iron wheel. It was replaced with rubber due to problems in the wear scar and abrasive breakage [33]. Returning to a steel wheel permits higher force loads and more effective abrasive agent breakage, as well as changes in the way in which the abrasive material moves through the contact surface between the primary surface and counter-surface. This has caused some trouble for the usage of these results in systems with complex phases. Gates, Gore *et al.* identified problems with using the SWAT in steels reinforced with coarse second phases, where anomalous results are seen with these materials, due to effects on the second phases [12]. However, Gore and Gates present an impact-abrasion test device with a remarkably similar construction and satisfactory results in other publications, though they once again show somewhat anomalous results in hard, carbide-

reinforced second phases [30]. With this caveat against use in certain materials, the SWAT appears to be able to be employable in the replication of high-stress three-body wear.

The scar produced in the surface of the sample can be analysed to study the interactions which occurring during the abrasion incident. The morphology of the scar will reveal the processes which occurred [34].

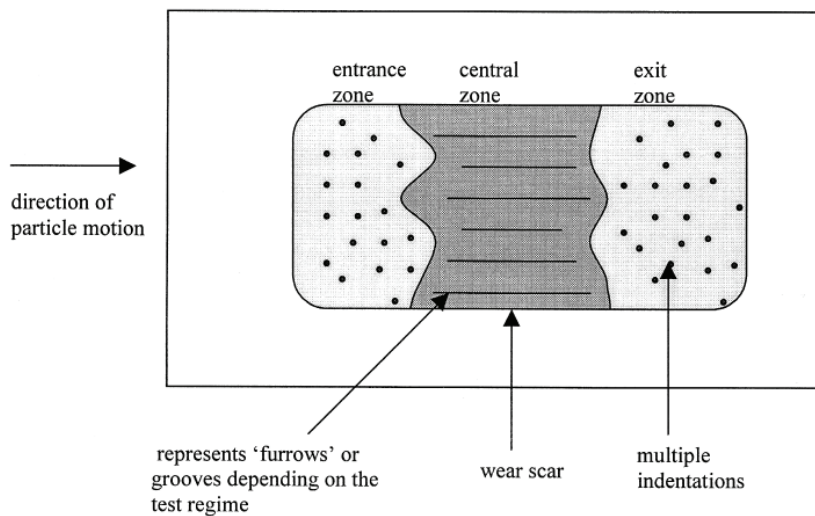


Figure 2-15: Wear scar schematic[34]

The indentations produced by the abrasive particles, as well as the grooves, furrows and scratch marks, can be traced to different wear mechanisms [34].

2.3.5 Decoupled wear model

To account for the full spectrum of mass loss occurring in a tumbling comminution mill such as a ball mill, the entirety of the degradation processes occurring there-in must be accounted for. Modern computational techniques now permit computer simulations of the motion of the charge inside a mill, using a technique called Discrete Element Method (DEM) This means that the

interactions occurring in the mill can be calculated and quantified for both frequency of given interaction event conditions and the forces occurring during those events [9-11, 28, 52-55]. From basic principles, it can be seen that the total mass lost in a system is the sum of the mass lost in each incident, which depends on the nature of those incidents and the amount of energy with which they occur. According to Radziszewski, the overall mass loss process can be represented as the sum of the individual processes according to the formula

$$\dot{m}_{total} = \sum_{i=1}^{n_{abr}} \dot{m}_{abr\ i}(E_{abr\ i}) + \frac{\dot{m}_{corr}}{A_{lball}} A_{rball} + \sum_{j=1}^{n_{imp}} \dot{m}_{imp\ j}(E_{imp\ j}) \quad \text{Eqn. 10}$$

where \dot{m}_x denotes the mass loss rate for a given process x , A_{lball} denotes the area of laboratory balls for corrosion tests, A_{rball} denotes the area of real mill media charge, E_{xy} denotes the energy dissipated for a given interaction x for a given system y , and the subscripts abr , $corr$ and imp denote abrasion, corrosion and impact, respectively [11]. Each contribution to the total mass loss can then be computed separately. Impact can be simulated using commercially available impact testing devices calibrated to replicate the energy and force regimes calculated by the DEM model. Corrosion values can be measured using static and dynamic corrosion tests. Abrasion processes then remain to be quantified and applied to the model. Abrasion can be initially described using Archard's relation, seen in Eqn. 8.

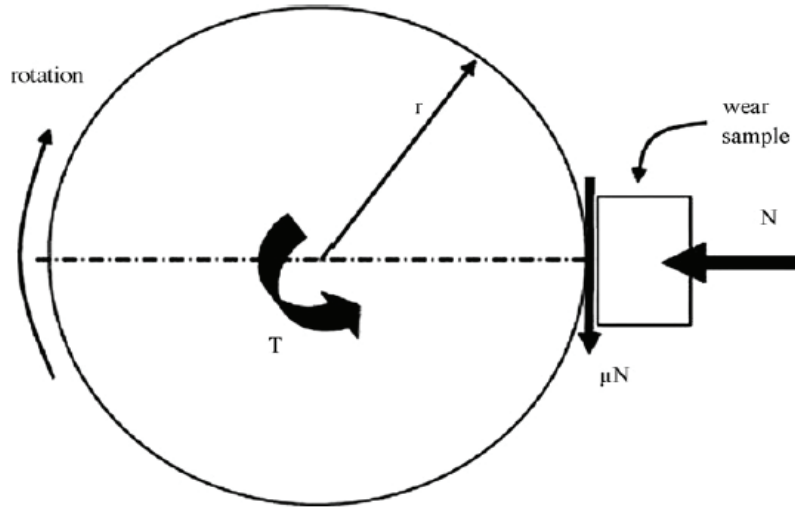


Figure 2-16: SWAT wheel free body diagram[39]

From the free body diagram of the abrasion system, seen above, the normal force can be related to the force by the frictional relationship

$$T = \mu \times F_N \times r \quad \text{Eqn. 11}$$

where T is the torque, μ is the frictional coefficient, F_N is the normal force and r is the wheel radius. The abrasive system can be simplified to an energy basis into

$$m_{abr} = k_1 \times E_{abr} \quad \text{Eqn. 12}$$

where k_1 is a proportionality constant in kg/J and E_{abr} is the abrasion energy [28].

From this, Archard's relation seen previously in Eqn.8 can also be restated on an energy basis, according to the form

$$m_{abr} = \rho \frac{\tan(\theta(N))}{\pi H_r} \mu N x \quad \text{Eqn. 13}$$

where $\tan(\theta(N))$ is a normal force dependant abrasion angle parameter [28]. This modified version of Archard's relation has been used by Radziszewski and others to account for the abrasive wear component in tumbling mills, and has been shown to be effective [8, 20, 28, 39, 56].

2.4 Degradation mitigation in comminution equipment

Due to the cost of grinding media, various approaches have been attempted to reduce media degradation. The first approach is to increase the wear resistance of the material. This is primarily accomplished by increasing the hardness of the media, through material selection [4]. In tumbling mills, this usually results in the selection of hard cast irons and steels. A hard surface will generally result in high wear resistance. Alloy selection must be carried out quite carefully, however, as some very hard steels are quite vulnerable to corrosion. Stainless steel or chrome-rich cast irons can be employed alleviate the corrosion [4]. Ceramic grinding media have been employed when the process stream is critically sensitive to iron contamination. Ceramics have the advantages of being chemically inert, as well as corrosion and wear resistant. However, certain drawbacks prohibit wide deployment. Ceramic grinding media can be much more expensive than metallic media of similar size and effect. They can also be much more vulnerable to high impact forces, which can cause chipping, cracking, or wholesale destruction [4]. Ceramics have therefore been restricted primarily to small mills, where impact forces are reduced. Material selection for grinding media will depend on the size of the mill, the ore processed, the environmental parameters inside the mill, as well as cost and the operator preferences and experience. The complexity of the wear often means that grinding media selection is often carried out *ad hoc*, on a strictly cost per ton of media basis, instead of on a lifetime cost.

Other degradation mitigation techniques depend on altering the design of the comminution mills themselves to reduce material degradation. Autogenous mills use the ore charge itself to induce comminution. These mills are built larger than equivalent ball mills. Large ore particles are tumbled in the mill, breaking themselves and other particles, through the forces generated by their own motion. Semi-autogenous mills rely on the same principle, adding some metallic charge media to facilitate the process. The use of these mills depends on processing requirements, as well as available funding. These mills are more expensive to purchase than ball mills, and require more energy [4].

2.5 Summary

In this chapter, the relevant scientific literature was examined, to acquire an understanding of the processes of comminution and wear. Comminution was first studied, as the process by which the size of ore particles is reduced by various pieces of equipment to induce particle breakage. One particular class of equipment, the tumbling mill, was described in detail, as were various means to evaluate comminution and breakage. Wear was then investigated, along with its mechanisms. Abrasion, the wear process caused by the motion of abrasive particles against a surface, was of particular interest, due to its influence in comminution systems. This process was studied in detail, models used to describe it were discussed and techniques used to measure it were studied.

Chapter 3 Methodology

This report section will describe the equipment employed during the present research, the principles upon which that equipment operates and the test materials used. The parameters and parameters employed will be discussed, as will some of the challenges faced.

3.1 Introduction

The techniques described in this thesis were carried out by the author in university facilities. The abrasion tests were carried out on a SWAT rig, using abrasive materials and metal samples selected to be of research interest.

3.2 Steel wheel abrasion test

The Steel Wheel Abrasion Test device used in this experiment was fabricated in-house in the Department of Mechanical Engineering at McGill, and is the third version of this apparatus in use in the Comminution Dynamics Laboratory.



Figure 3-1: SWAT apparatus, Version 3 (left) CAD design, (right) apparatus

In construction, the machine is similar to the standard setup described in ASTM G65. The standard specifies a 9” chlorobutyl rubber-coated steel wheel, while the SWAT test uses a solid steel wheel with an 11” diameter. The wheel rotational speed is also variable, set by the variable speed drive and the motor control unit. The force applied to the sample is determined by the weights selected in the weight stack. Finally, and perhaps most importantly, a Binsfeld Engineering full bridge torque gauge has been affixed to the shaft linking the motor unit and the steel wheel. This gauge measures the strain experienced by the shaft, which is then wirelessly transmitted to the Data Acquisition System affixed to a desktop computer for real-time data collection during the test. The signal received in volts, can be converted to a torque value in Nm, which permits force and energy calculations. Therefore, the actual force and energy input into the system can be determined.

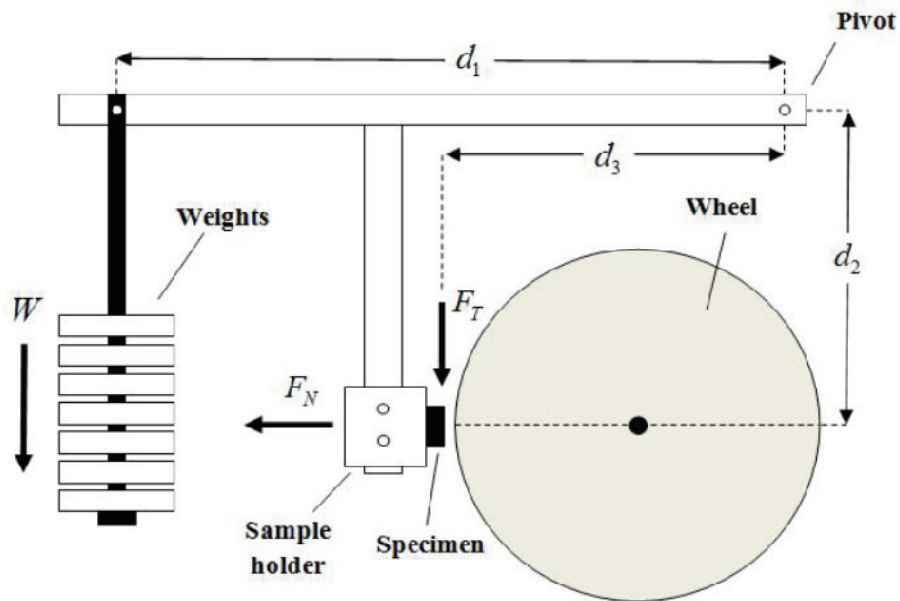


Figure 3-2: SWAT Sample application system and force diagram[56]

The normal force applied to the sample, F_N , is determined by the weight selected on the weight stack, W , the lever arm lengths d_1 , d_2 and d_3 , the wheel radius r and the force applied by the wheel F_T . This force, applied by the wheel, can be calculated from the torque measured by the strain gauge according to

$$F_T = \frac{T}{r} \quad \text{Eqn. 14}$$

The lengths d_1 and d_3 are fixed, while d_2 is adjustable as needed to ensure a proper sample/wheel contact surface. The wheel radius can be measured, and W is one of the selected test settings. F_N can then be calculated from the free body diagram.

$$F_N = \frac{1}{d_2} \left(W \times d_1 + \frac{T}{r} \times d_3 \right) \quad \text{Eqn. 15}$$

This implies that with changes in torque in the system, there will be some alteration in the force experienced by the sample. This is consistent with problems identified in early versions of ASTM G65, when the pivot point is not in line with the sample surface, such that a moment is generated in the lever arm. This problem has been identified and rectified in later versions of the standard, but persists in the current version of the SWAT apparatus used. A correction can be applied to determine the true normal force discussed above.

Power input into the system can be calculated from the applied torque and the rotational speed of the wheel. The power can then be represented as

$$P = \bar{T} \times \omega \quad \text{Eqn. 16}$$

where \bar{T} is the average torque over the test duration and ω is the rotational speed.

3.3 Material selection

Abrasive materials were selected according to current SWAT guidelines and our research interests. The current standard abrasive used is Ottawa Foundry Sand, commercially provided by Opta Minerals under the trade name Barco 32. As one of the parameters of interest was abrasive particle size, two other abrasive materials with smaller sizes were also initially selected: Barco 71 and Barco 125. Barco 125 was later discarded from research as it was too fine to flow properly and could not be used effectively without significantly altering the SWAT apparatus setup and procedure. The abrasives were supplied as commercially packaged 25 kg bags. Sample composition was SiO₂ at 99.0% and up, with trace Al₂O₃, Fe₂O₃ and TiO₂ at less than 1.0% total [57]. Bagged charges were combined and blended amongst the same classes to ensure a consistent distribution within a class. Samples were riffled out for measurements. The size distribution of the material is given below in Table 3-1, as measured according to the procedure outlined in Section 3.7, matching commercial specifications.

Table 3-1: Abrasive material size distribution by percentage

Screen Size		Distribution in Barco 32 (%)	Distribution in Barco 71 (%)
Tyler Mesh	Size (um)		
30	600	5.05	0.00
35	500	24.81	0.00
40	425	39.86	1.48
50	300	28.08	12.06
70	212	1.91	39.03
100	150	0.25	33.66
140	106	0.03	11.81
200	75	0.01	1.78
270	53	-	0.14
Pan	0	0.00	0.03

Silica sand, with a fairly high hardness of 7 on the Mohs hardness scale, is an effective abrading agent [58]. Silica is an ideal abradant for experimental work due to its high presence in the Earth’s crust, which makes it near ubiquitous, and its high hardness, which means it is likely to be encountered as an abrasive agent in almost every potential industrial application, [59]. The silica materials used in these tests are also similar in composition and morphology to the material specified in the ASTM G65 standard [43].

For the metal samples, four types were selected for the test work: SAE-AISI 1018 low-carbon general purpose mild steel, SAE-AISI 4140 medium-carbon high-strength low-alloy steel, SAE-AISI 8620 low nickel-chromium-molybdenum carburizing steel and AISI 410 stainless steel[60, 61]. These samples were selected because they represent a wide classes of steel types, and are commercially available. Compositions of the steel samples are given in Table 3-2.

Table 3-2: Steel test material elemental composition ranges

Steel	C (%)	Cr (%)	Mn (%)	P max (%)	S max (%)	Si	Ni	Cr	Mo
1018 [60]	0.14- 0.20		0.60- 0.90	0.040	0.050				
4140 [60]	0.38- 0.43		0.75- 1.00	0.035	0.040	0.15- 0.35		0.80- 1.10	0.15- 0.25
8620 [60]	0.18- 0.23		0.70- 0.90	0.035	0.040	0.15- 0.35	0.40- 0.70	0.40- 0.70	0.15- 0.25
410 [61]	0.15	11.5- 13.5	1.00	0.04	0.03	1.00			

The steel samples were acquired from McMaster-Carr as 2.0” diameter, 6’ length steel rods. Test samples were cut down to a length of 1.50” using a Kalamazoo Industries 14” water-cooled abrasive chop saw. This saw is designed to provide a rapid, clean cut through metal pieces. Cuts were accomplished using 14” diameter resin-bonded abrasive cut off blades, model CW14-10, from Met Lab Corp. This model was selected for both cutting speed and accuracy in hard steels.

The four steel samples were tested for material hardness using an automated Mitutoyo WizHard HR-500, with a diamond indenter in the Rockwell A regime. Average values of hardness are given below.

Table 3-3: Steel sample hardness values

Sample	Hardness (HRA)	Standard Deviation
1018	50.9	1.2
4140	64.4	0.6
8620	51.7	3.2
410	50.8	2.5

Cast irons, as well as samples from actual comminution media, were not selected, due to problems with availability in sufficient quantity for the amount of tests required, as well as material consistency within each material type. Other tests have been carried out on actual comminution media in other sample campaigns, but are not listed here for the sake of brevity.

3.4 Experimental parameters

Two of the experimental parameters of interest were the wheel speed and the force applied to the sample. Wheel speed is set using the power supplied to the

SWAT motor. The standard used for experimental work is 150 RPM [62]. Three speeds were initially selected for use: 90 RPM, 150 RPM and 210 RPM. By altering the rotational speed of the wheel, the relative sliding speed of the interacting wheel and sample can be controlled. The selection of wheel speeds was altered during ongoing work, due to results seen in the first phase of the experiment. This will be discussed further in this paper.

The force applied by the wheel to the sample is determined by the weight applied to the lever arm holding the sample. When the sample is pressed against the wheel, the force is determined by the setting selected on the weight stack, modulated by the torque occurring at the interface. Five mass settings were selected for the machine, namely 10, 20, 30, 40 and 50 lbs. Through the action of the lever arm, these weights result in nominal applied forces of 50.43, 100.86, 151.29, 201.72 and 252.15 N, respectively. The influence of system torque, discussed previously in section 3.2, will slightly alter these values. Test time, as per standard, will remain 120 seconds. Each test is carried out a minimum of twice per experimental condition.

3.5 Test identification and nomenclature

Each test specimen was given an identification number MSS-FF-SP-N. *M* is the material type, with 1018 as “A”, 4140 as “B”, 8620 as “C” and 410 stainless as “D”. *SS* is the abrasive size, either “32” for Barco 32 or “71” for Barco 71. *FF* is the selected weight, 10, 20, 30, 40 or 50 pounds, *SP* is the wheel speed, 90, 150 or 210 RPM. *N* is test repeat number. All tests were carried out a minimum of twice per condition, with more executed if there was a problem with test results.

In this system, the test ID reference B32-40-150-2 would designate the second test carried out with 4140 steel, Barco 32 abrasive, a 40 pound load and 150 RPM wheel speed.

3.6 Experimental procedure

All Steel Wheel Abrasion tests were carried out using the current version the Comminution Dynamics Laboratory SWAT procedure, developed in house [62]. This is derived, as is the test itself, from ASTM G65 [43].

1. All equipment is verified to ensure proper functioning. Torque gauge battery charge is verified.
2. Torque gauge, sensor station and multimeter are activated.
3. A sample is cut, cleaned, dried and weighed.
4. The sample is installed in sample holder, with sample face flush to wheel surface.
5. Abrasive material is loaded into sample hopper.
6. The motor test speed is set into the variable speed drive controller.
7. A collection vessel is installed under the collection hopper.
8. The desired test force load is set.
9. The dust collection system is activated.
10. The test motor is started and allowed to come to set speed.
11. The Data Acquisition System is started when drive is at speed.
12. The DAS reading is adjusted until baseline torque reads as a signal of 0V.

13. Abrasive material is directed from the sample holder to the test nozzle, ensuring a steady flow through the nozzle, with a thin, uniform sand layer. The nozzle is fixed by fabrication to a flow of 300 g/min.
14. The lever arm is depressed and locked, loading the sample against the wheel. The start time is recorded.
15. After 120 seconds, the lever arm is unlocked and allowed to fall, stopping the test.
16. The SWAT motor and abrasive material flow are stopped.
17. The metal sample is allowed to cool, removed from the holder, cleaned and weighed.
18. Abrasive material present in the hopper is brushed into the collection vessel, recovered and labelled for size determination.
19. Test torque data is saved and analysed according to procedures outlined in Section 3.8.

3.7 Particle size determination

Abrasive materials were screened using a standard Ro-Tap sieving apparatus. The Barco 32 material was sieved using standard Tyler screens in the screen progression from 30 mesh (600 μm) to 200 mesh (75 μm). The Barco 71 material was sieved using the screens from 40 mesh to 200 mesh, along with the 270 mesh (53 μm). For both materials, screening was carried out for 15 minutes. For the Barco 32, the whole sample was loaded into the Ro-Tap at once, while for the Barco 71, the charge was split in half, and run as two separate passes to ensure proper reading and minimize blinding effects on the screens. The separate

fractions were then weighed and measured to calculate the size distribution of a given sample.

3.8 Torque data processing

Torque values are transmitted from the torque gauge to the wireless DAS, which registers the values as a voltage at a given time. These values can then be plotted and analysed.

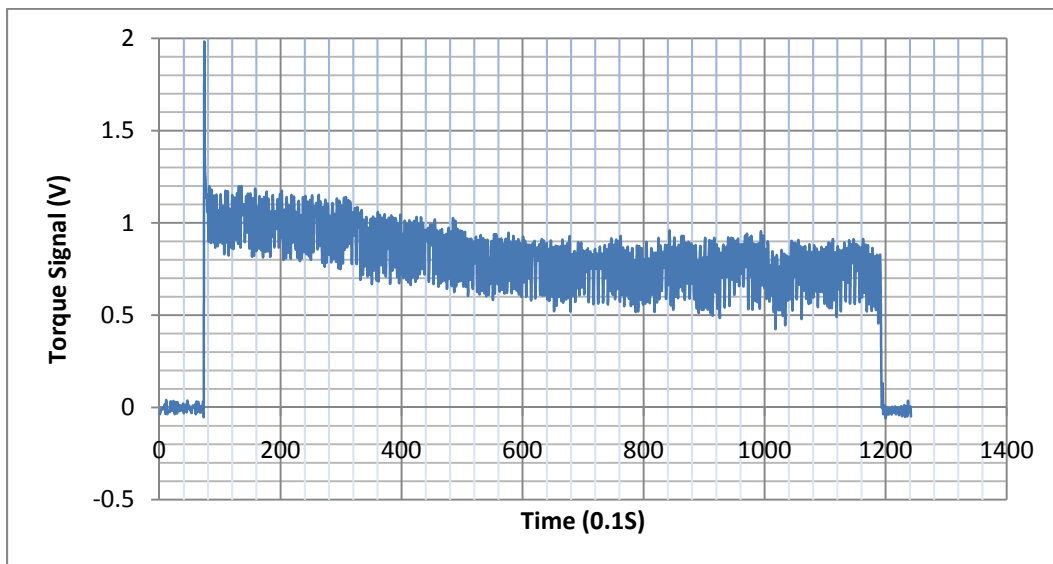


Figure 3-3: Sample torque voltage graph, test D32-30-150-2

The torque value for the test is calculated by taking the average during the test, in Figure 3-3 between 7.3seconds and 119.3 seconds, and subtracting the baseline torque, before 7.3 seconds and after 119.3 seconds. This yields the average torque value during the test, in volts. This value is then converted to Nm through known conversion factors for the system.

3.9 Experimental methods modifications

Certain experimental parameters were abandoned. After visual inspection of wear scars, it was found that during the 210 RPM tests, the wheel speed was

too high. This meant that too little abrasive material was entrained into the interfacial contact area. Surface analysis of the wear scar showed that the sample entered two-body wear, instead of the three-body regime desired. The 210 RPM test was therefore terminated. During test work on the 410 stainless steel, catastrophic equipment failure in the system drive coupling lead to the loss of over 40 test sample results. The entire series of 410 samples had to be reprocessed. For the subsequent testing in the 4140 and 8620 steels, the 90 RPM test were abandoned due to time constraints.

This damage was caused when a key lock, joining the drive transmission to the wheel shaft slipped partially from the keyway. It remained partially lodged and constrained in the joint, due to the presence of a polymer linking collar. The drive shaft and coupling were warped and twisted by the presence of the key. Due to the hidden nature of the damage, it was not uncovered until a detailed data analysis. Torque values recorded during the tests appeared somewhat erratic, but tolerable at first glance. Upon closer analysis, however, the results were unreliable. The SWAT apparatus was then disassembled and the damage discovered. The machine was repaired and the unreliable data discarded.

3.10 Summary

In this chapter, the experimental apparatus and procedures used for the present work were described and detailed. From this, it was possible to develop procedures to replicate abrasion and comminution in a test process.

Chapter 4 Results and Discussion

The present section of the report will express the results obtained during the previously described experimental work. The surfaces of the wear scars will be analysed to observed the impact of wear. The abrasion process will then be studied with regard to the applied forces and work on the system. Specific energy metrics will be used and compared to further study abrasion and comminution, attempting to link the two phenomena.

4.1 Wear scar characterisation and analysis

The first component of wear analysis, both in the SWAT technique and in any other tribological wear testing technique, is surface analysis of the wear scar. Figure 2-15 shows the characteristic scar produced by the SWAT. By studying these scars, certain details may be gleaned from the pattern.

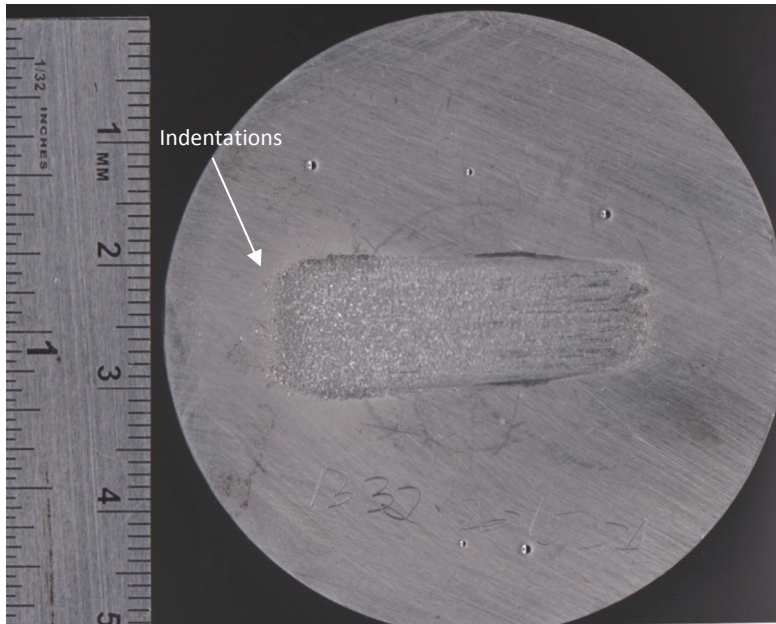


Figure 4-1: Sample B32-20-150-1

Pictured above is a typical wear scar with a 150 N load, in 4140 steel with Barco 32 as the abrasive, with wheel rotation from left to right. On the leftmost side of the scar, indentations can be seen. This type of pattern is more visible in Figure 4-2.

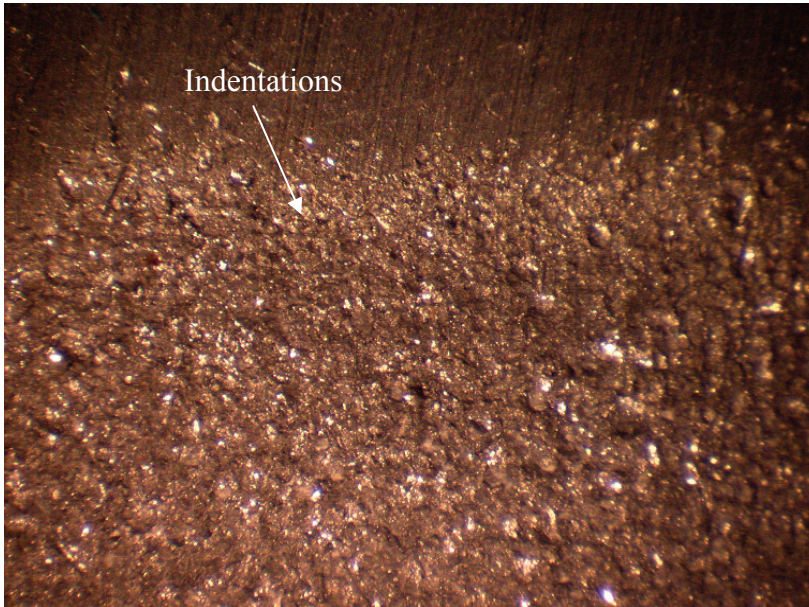


Figure 4-2: Sample A32-20-90 wear scar, top view, 2X magnification

These indentations occur from abrasive material pushed into the primary surface, causing deformation and wear. Further down the wear scar, as the abrasive agent is dragged along causing scratches and grooves, as in Figure 4-3

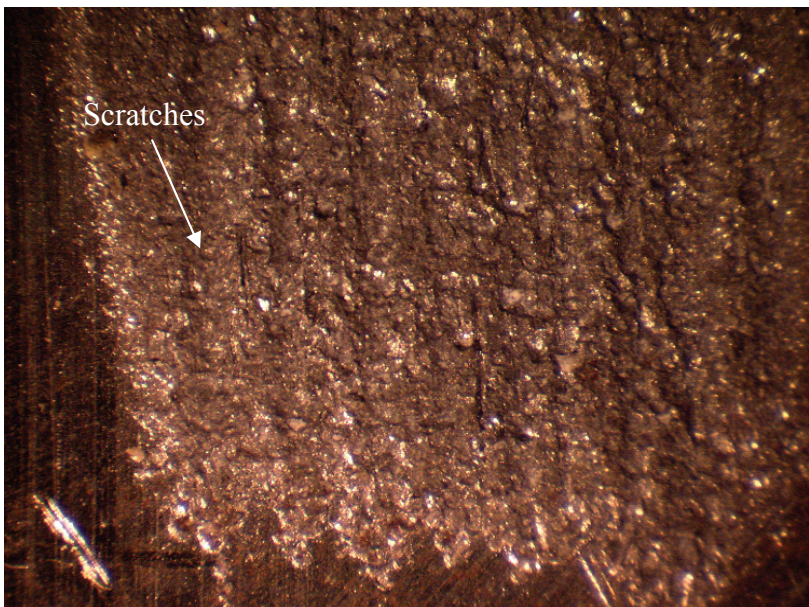


Figure 4-3: Sample A32-20-90, bottom view, 2X magnification

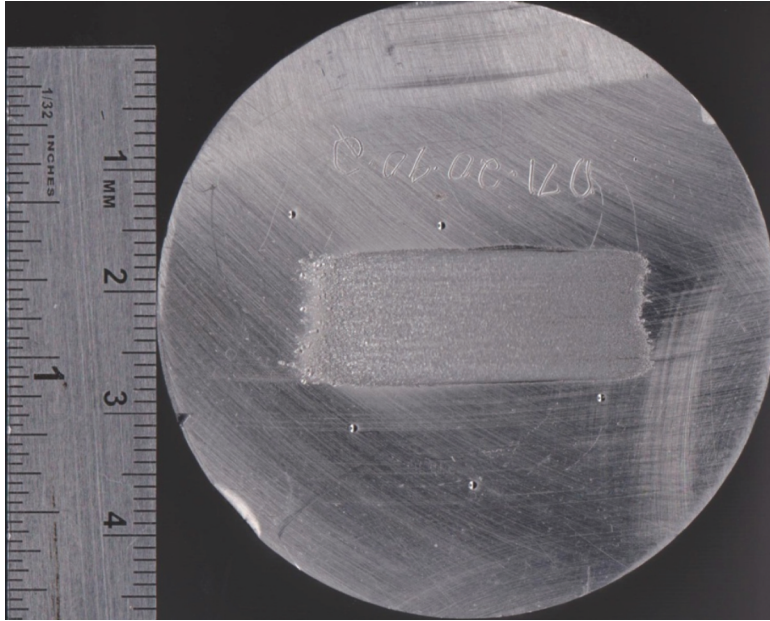


Figure 4-4: Sample D71-20-90-2

Barco 71 abrasive induced many of the same wear patterns as Barco 32 in the material, as can be seen in Figure 4-4, once again left to right, though many of the wear features are finer grained, naturally, due to the smaller abrasive size. One feature which occurred only in the tests with the coarser Barco 32 was the presence of sets of significantly deeper and more pronounced grooves in the surface of the wear scar, as seen in Figure 4-5 and at higher magnification in Figure 4-6.

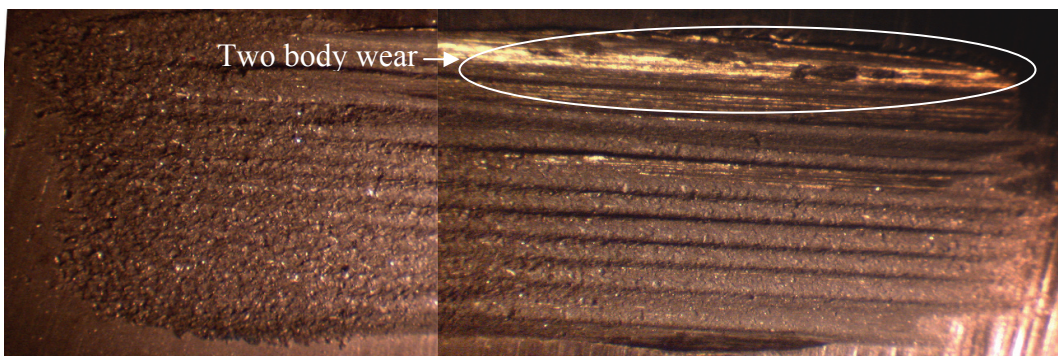


Figure 4-5: Sample A32-20-210, 2X magnification, digitally stitched

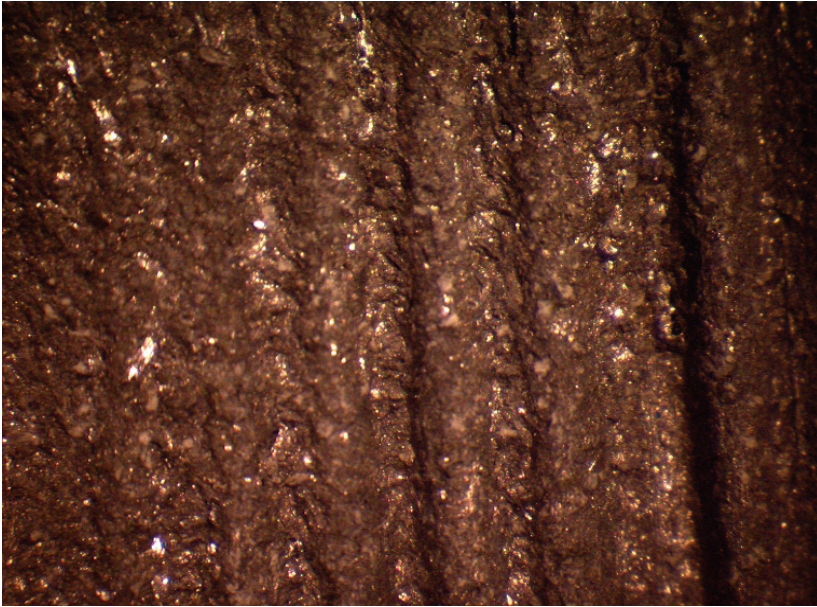


Figure 4-6: Sample A32-20-210, Middle view, 3X magnification

This wear pattern, which has been referred to as channelling within the Comminution Dynamics Laboratory, was seen only in wear scars caused by Barco 32. Found in all tests with Barco 32, channels are long grooves starting approximately a third of the way into the scar, increasing in depth and size down the wear track. Channels also increase in severity with increasing applied force on the sample. The channels have a size on the same order as the Barco 32 abrasive. The mechanisms for channel formation is not yet fully determined, but it is likely that channelling occurs because abrasive grains of Barco 32 form initial scratches and subsequent grains follow in that pre-existing scratch, instead of starting a new one, which would require more energy.

Figure 4-5 also reveals another element of note in wear scars and the reason testing at 210 RPM was abandoned, as discussed in Section 3.9 of the methodology. Along the top of the wear track seen in Figure 4-5, the wear scar is

smooth, shiny and devoid of the scratching and grooving caused by three-body abrasion. This was even more apparent at higher magnification, as can be seen in Figure 4-7.



Figure 4-7: Sample A32-20-210, Side view, 3X Magnification

This shiny, smooth surface is characteristic not of three-body wear, but of two-body wear, such that it is caused by direct metal-on-metal contact. Similar patterns were seen in all tests at 210 RPM. In these tests, at the set abrasive flow rate of 300 g/min, there was a problem in the movement of abrasive material through the wear region. The speed of the wheel was so high that abrasive grains were rejected from the contact. The abrasive grains were not entrained by the wheel against the steel surface, leading to abrasive grain depletion in the contact and metal-on-metal wear. This is consistent with known particle entrainment behaviour in three-body systems [63].

Two-body wear was also seen in the channelling occurring in Barco 32 at high applied force loads, as discussed previously. The regions between channels often have the same shiny appearance, indicating that some degree of two-body wear, requiring direct metal-on-metal contact, occurs in the raised sections between the deep channels. This requires that abrasive material either pass in the channel or be expelled from the side of the contact region without abrading the surface. This supplies evidence supporting the belief that the channels act as pathways for abrasive grains through the contact region, such that the grains bypass the contact area by using and enlarging initial scratches.

4.2 Wear as mass loss response

Wear was first measured as a mass loss of the sample following the test. It was therefore reported, at least initially, as the mass lost to the abrasion incident as a function of the force applied for the different test circumstances. Figure 4-8 shows the mass lost to wear in 1018 steel, for three rotational speeds, 90, 150 and 210 RPM, for both the Barco 32 and the Barco 71 abrasives. This system shows interesting behaviour. For the coarse abrasive, the three systems maintain similar force loads and mass loss until the third test point, approximately 240 N, where they then diverge. The 90 RPM maintains a steady mass loss for all other loads. The 150 RPM system mass loss response lowers with increasing force, while the 210 RPM system first drops slightly and then climbs dramatically. This behaviour in the coarse abrasives can be explained in terms of abrasive agent rejection at high applied contact forces and wheel speeds. In these high force systems, a

greater amount of material is rejected from the abrasive interface, leading to metal-on-metal contact. This was seen in the surface analysis carried out previously. At higher wheel speeds, material is rejected from the contact area, increasing the amount of two-body wear, which will induce less mass loss. This can account of the drop in mass loss experienced by the 150 RPM and 210 RPM systems. The final increase in mass loss seen in the 210 RPM at the highest forces is likely due to the very high forces, inducing excessive wear. These systems also see very high levels of channelling occur. At very high forces, this induces high wear in the channel regions.

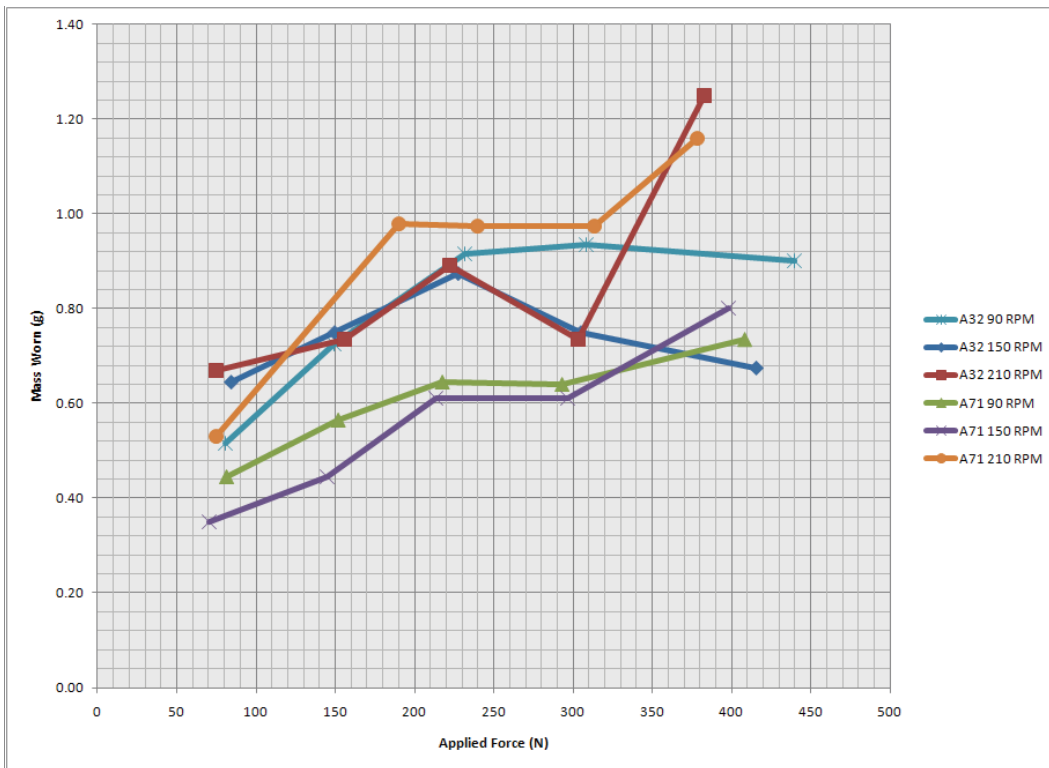


Figure 4-8: Mass loss in wear as a function of applied force, 1018 Steel

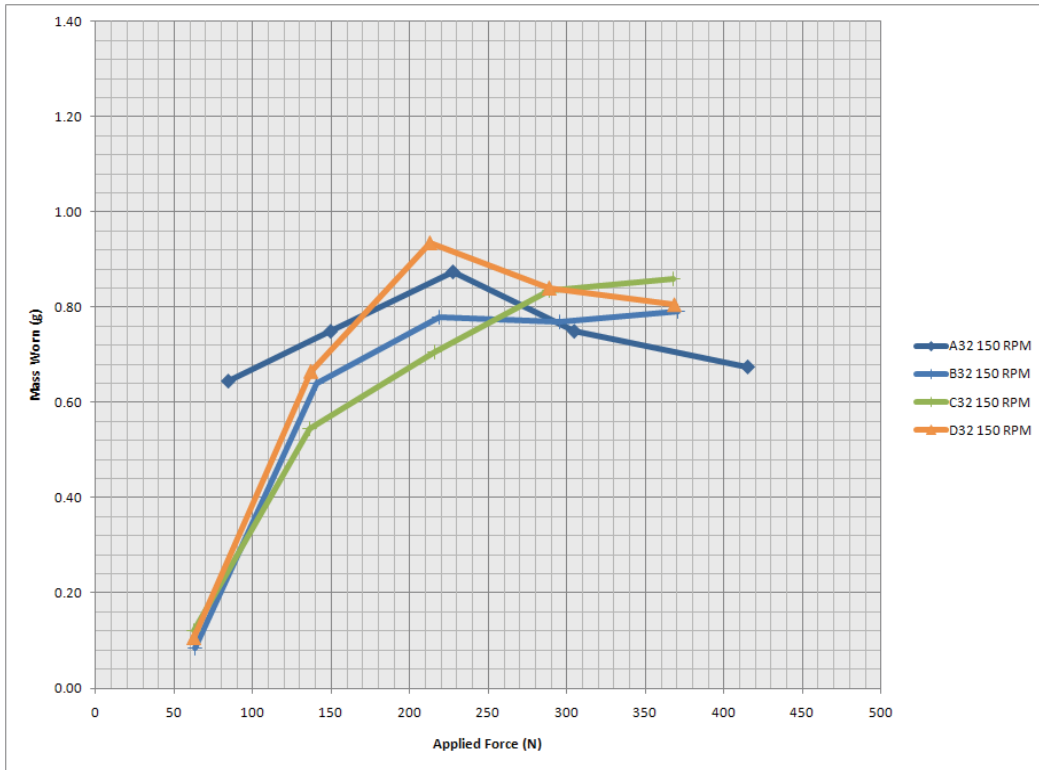


Figure 4-9: Mass loss in wear as a function of applied force, 150 RPM, Barco 32 abrasive

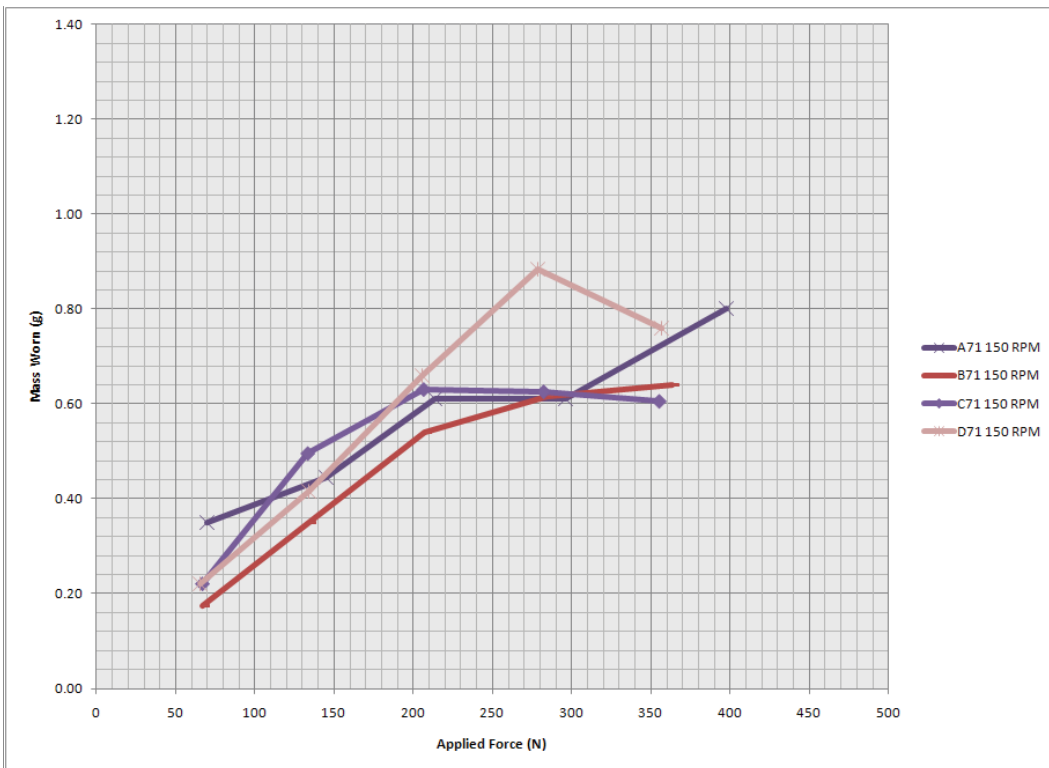


Figure 4-10: Mass loss in wear as a function of applied force, 150 RPM, Barco 71 abrasive

In the tests with fine abrasives, the systems appear to be better behaved. For all three rotational speeds, the wear response increases with increasing force. The 90 and 150 RPM systems have a close level of wear, while the 210 RPM system experienced much higher wear as an absolute mass loss.

Figure 4-9 and Figure 4-10 show the mass loss in all four steel samples tested at 150 RPM. These show similar behaviour to that which occurred previously. In the majority of cases, the wear response increases with increasing force. For Barco 32, wear decreases after approximately 250 N for the 1018 and 410 steels, while in the Barco 71, wear decreases for the 410 stainless only.

The general trend, however, is consistent with previous literature, where the wear response increase sharply with increasing force in the lower force regions, levelling off at higher regimes. In absolute terms, the highest wear is seen in the 410 stainless steel, for both the coarse and fine abrasives.

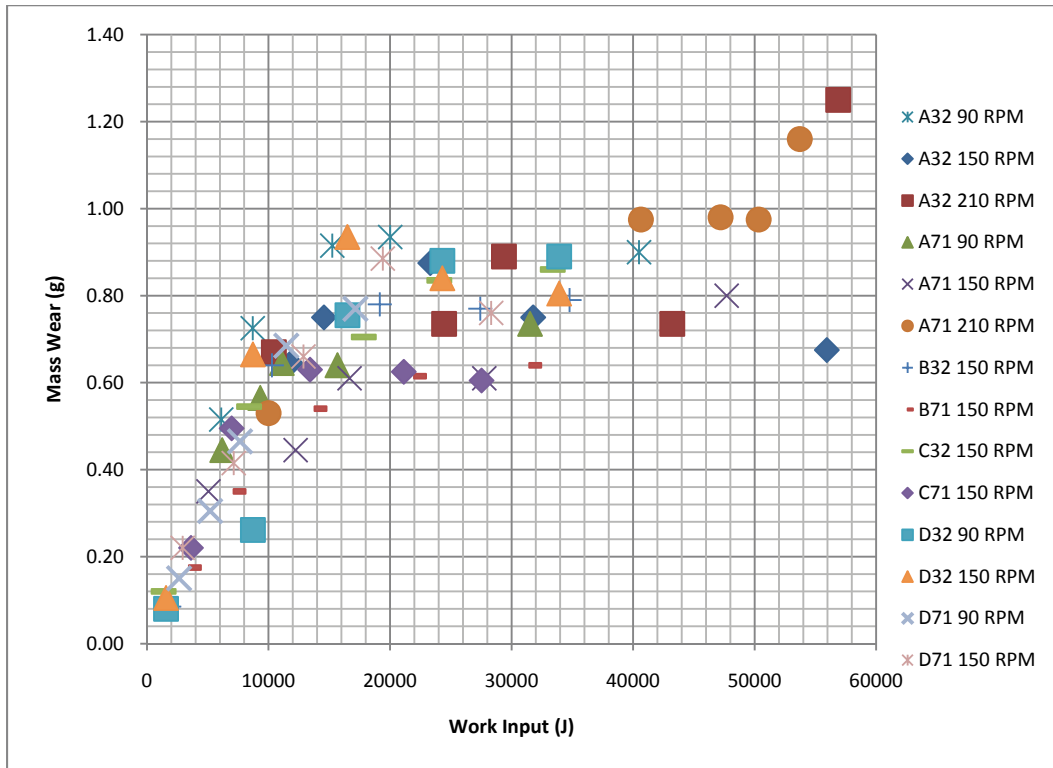


Figure 4-11: Mass loss in wear as a function of work input

Figure 4-11 shows the mass loss as a function of work input into the system. The energy term is derived from Eqn. 16, seen in the methodology, where power is calculated as the product of the average torque and the wheel rotational speed. Multiplying the power by the test duration t yields the work input into the system, W_T , which can later be used for specific wear and specific breakage.

$$W_T = P \times t = \bar{T} \times \omega \times t \quad \text{Eqn. 17}$$

The energy dependency is more apparent in Figure 4-11 than in the earlier figures strictly showing wear as a function of force. The system torque is more complex than simply being dependant on applied force. The torque depends not only on the applied force, but also on the wheel rotational speed and the abrasive material used. All of these will therefore influence the work done on the sample during the

abrasion incident. In a system such as this, the energy input is consumed by the different processes, such as abrasive wear, abrasive agent breakage and heat generation. In this analysis, consumption of energy by heat has been assumed negligible. Very little change in temperature was observed during testing in the various abrasive configurations.

4.3 Specific abrasion energy

The wear occurring in a system can be related to the amount of work being put towards an abrasion event. The abrasion incident can therefore be quantified on a mass loss per unit of energy basis. This enables the calculation of a specific abrasion energy for a given abrasive incident. This is done by first evaluating the abrasive work in a system, which is given by the total work multiplied by the friction coefficient. This is used to divide the mass of metal lost in an abrasion incident to generate the specific energy, as per the formula

$$E_{AS} = \frac{m_{abr}}{\mu W_T} \quad \text{Eqn. 18}$$

where E_{AS} is the specific abrasion energy in kg/kWh, m_{abr} is the mass lost to abrasion, μ is the friction coefficient and W_T is the work input. This parameter is interesting as it can be employed in DEM modeling to compute the wear occurring in a given interaction, for known system conditions.

Using these equations, the specific abrasion energy was calculated for each abrasion incident occurring during the tests. This can provide great insight into what is occurring during the abrasion process. The results of these

calculations are shown in Figure 4-12, Figure 4-13 and Figure 4-14. These figures show the specific abrasion as function of the force applied during the test, much like in earlier figures showing absolute wear.

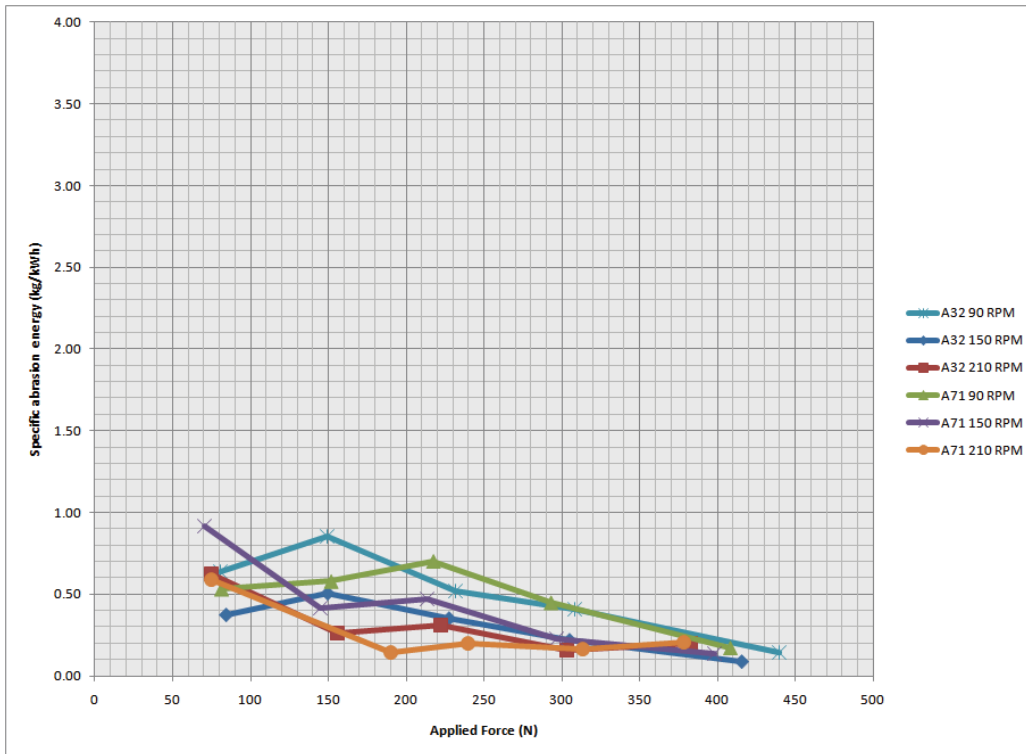


Figure 4-12: Specific abrasion energy as a function of applied force, 1018 steel

Figure 4-12 shows the specific abrasion energy for the tests occurring in 1018 steel, with coarse and fine abrasives. In this system, while overall specific wear values are low, trends are readily visible. The specific abrasion energy decreases with increasing force in all systems. In most cases, the 90 RPM system has the highest specific wear energy for a given force. While divergent at low forces, the specific abrasion values eventually cross and joint at higher forces. The 150 RPM system starts at low forces with very divergent levels of specific abrasion energy, but these also converge at higher forces. At 210 RPM, the

system starts with convergent values for the specific abrasion energy and maintains convergence throughout. The 210 RPM system has the lowest specific abrasion energy throughout the majority of the test. The faster systems have a higher total work input, but their specific abrasion energy decreases with increasing wheel speed and force. The amount of energy going into a given system is increased with higher wheel speeds and applied forces, but the effectiveness of that input work in causing abrasive wear is reduced.

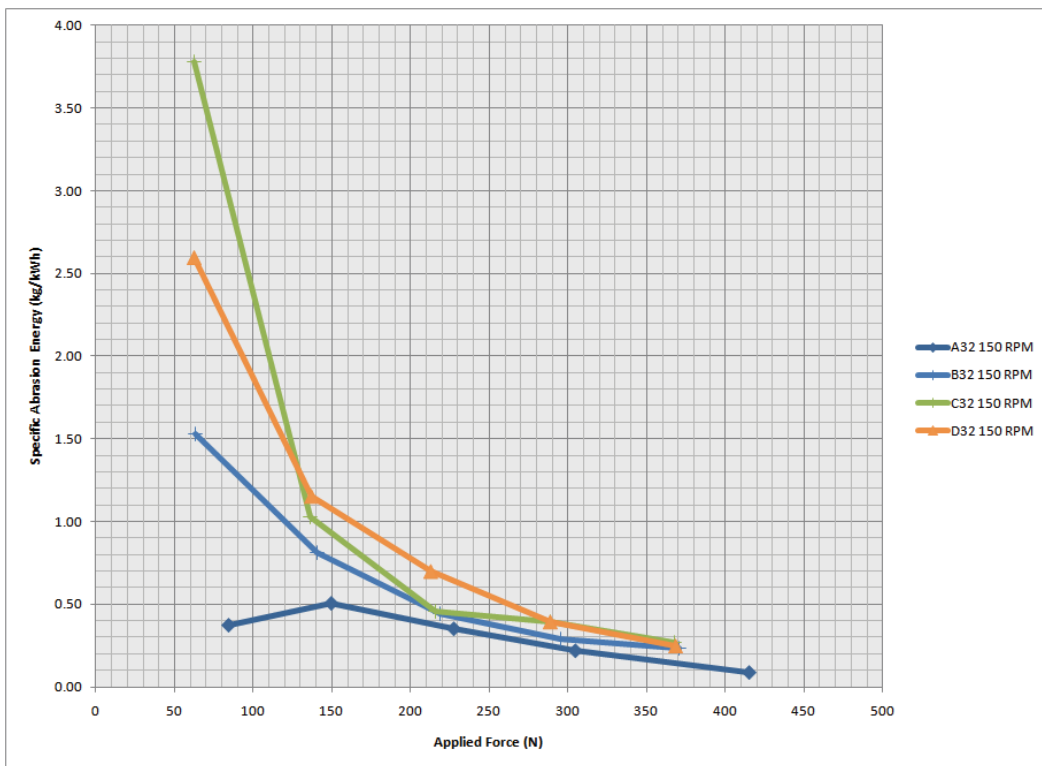


Figure 4-13: Specific abrasion energy as a function of applied force, 150 RPM, Barco 32 abrasive

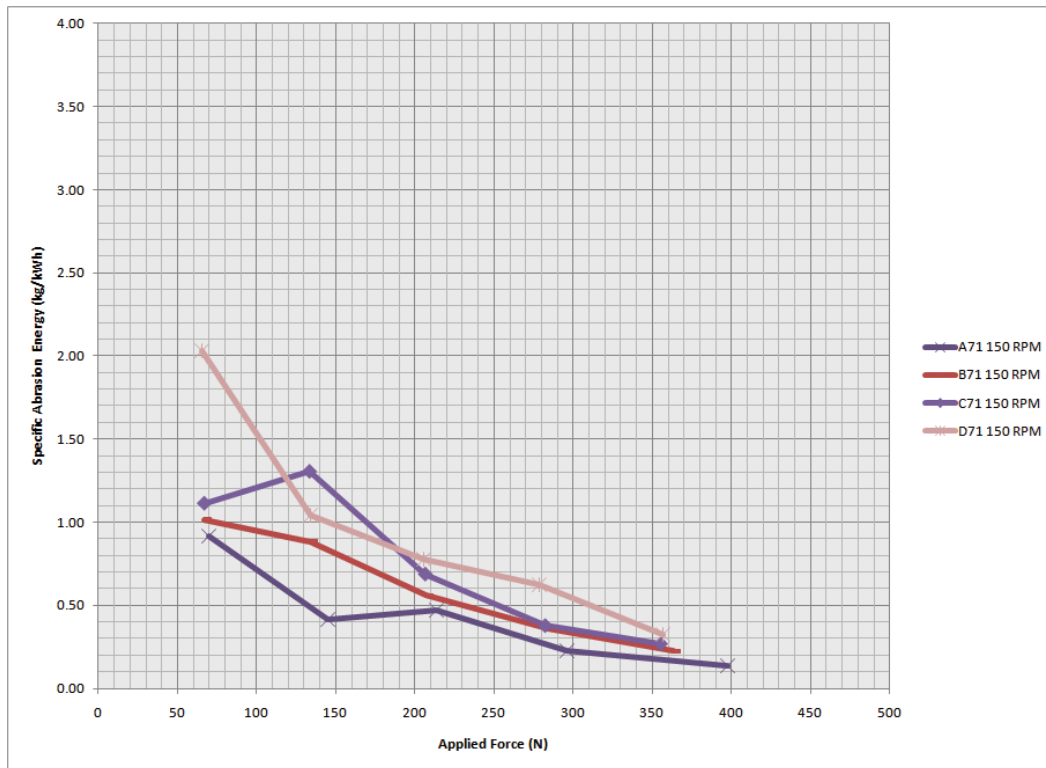


Figure 4-14: Specific abrasion energy as a function of applied force, 150 RPM, Barco 71 abrasive

Figure 4-13 and Figure 4-14 show the specific abrasion energy as a function of applied force for the 150 RPM tests, in all four steels tested. The first and most readily apparent feature is the very high specific wear seen in the 8620 steel system, classified as the “C” series of tests, for both the coarse and fine abrasives. Generalities can still be drawn from the system. As before, the specific abrasion energy is high at low forces, dropping steadily as the force increases. The 1018 steel, “A” class, behaves as described previously, starting diverged and converging at medium force levels, while dropping with increasing force. The same holds true for the 4140 steel. The 8620 steel offers the most complex response. At the lowest force, the 8620 with the Barco 32 has the highest specific abrasion wear of any set of test conditions, while the test with Barco 71 is much

lower. At the lowest force increment, the situation has changed. The specific abrasion energy for the coarse abrasive has dropped to below the specific abrasion energy of the fine abrasive, which has increased. This ranking continues for the next few force increments, all while the specific energy itself drops, until the values converge at high forces. In the 410 stainless steel, the “D” class, the values are once again quite high, this time for both of the abrasive types. Specific abrasion wear values drop with increasing force, meeting the other systems at higher force levels. Once again, increasing applied forces, while increasing the work input into the system, is less effective at inducing abrasive wear. As seen in Figure 4-9, Figure 4-10 and Figure 4-11, the mass lost in abrasion increases with increasing applied forces and work. The specific abrasion energy decreases, however, showing that this increased work is less effective at inducing abrasion

Figure 4-12, Figure 4-13 and Figure 4-14, along with the specific abrasion energy parameter itself, offer a complex view of the abrasive system. The high values in the 8620 and 410 steels are initially quite puzzling until one looks at the equations describing the system. Equations 11, 17 and 18 show that the specific abrasion energy parameter E_{AS} depends on the torque supplied to the abrasion event.

$$E_{AS} = \frac{m_{abr}}{\mu W_T} = \frac{m_{abr}}{\left(\frac{T}{F_N \times r}\right) T \times \omega \times t} = \frac{m_{abr} \times F_N \times r}{T^2 \times \omega \times t} \quad \text{Eqn. 19}$$

For the experiments conducted in the 1018 steel, the wheel speed, radius and test time have been maintained constant. Thus, the variables that influence specific abrasion energy are the sample mass lost to abrasion, the applied force and the

torque value squared. Studying two similar systems yields an explanation. The 4140 and 8620 steels with Barco 32 abrasive have specific abrasion energy vs. applied force curves that follow a similar shape, as seen in Figure 4-13. However, 8620 steel does not have high values of E_{AS} , unlike 4140. Looking at the numbers in this case, as shown in Table 4-1, reveals what is occurring.

Table 4-1: Specific abrasion energy values for B32 and C32 systems

Sample ID	Mass loss (g)	Applied force (N)	Torque (Nm)	Friction coefficient	E_{CS} (kg/kWh)
B32-10-150	0.09	63.3	0.97	0.11	1.53
B32-20-150	0.64	140.6	5.46	0.28	0.81
B32-30-150	0.78	218.7	10.16	0.33	0.44
B32-40-150	0.77	295.6	14.55	0.35	0.29
B32-50-150	0.79	370.5	18.45	0.36	0.23
C32-10-150	0.12	62.3	0.73	0.08	3.78
C32-20-150	0.55	136.6	4.46	0.23	1.03
C32-30-150	0.70	215.9	9.46	0.31	0.46
C32-40-150	0.84	288.4	12.76	0.32	0.40
C32-50-150	0.86	367.6	17.72	0.34	0.27

While the applied force values are nearly identical between B32-10-150 and C32-10-150, the mass loss and torque values are not. The “C” class test loses more mass, but reports a lower torque. The low torque values seen during the low force tests lead, as implied by Eqn. 19, to high E_{CS} values.

4.4 Specific comminution energy

Much as the abrasive wear occurring in the experiment can be quantified as a portion of the input work into the system, the same holds true for the breakage occurring in the abrasive agents themselves, which can also be quantified. The breakage of the abrasives with regard to the energy input can be

used to determine how effectively comminution and breakage occur with increasing energy input. This parameter is hoped to be used in DEM modeling, where it could be employed to calculate the comminution occurring for a given interaction, knowing the system conditions of that interaction,

The first step in carrying out this analysis is measuring the breakage occurring in the abrasive agents. Knowing the average initial particle size distribution of the material before abrasion and having screened the material after abrasion, the mass of broken material can be calculated from the formula

$$m_{bk} = \sum_{i=1}^n m_{i \text{ final}} - m_{i \text{ initial}} \quad n < j \quad \text{Eqn. 20}$$

where m_{bk} is the broken ore mass, $m_{i \text{ final}}$ is the mass of the size interval i after breakage, $m_{i \text{ initial}}$ is the mass of the size interval i before breakage, i denotes the size class below the original size interval j [21]. Knowing the amount of breakage occurring and the work supplied to the system, the specific comminution energy can be calculated. This term, E_{cs} , is structured in the same manner as how it is used in the context of the t_{10} test, as described in Eqn. 2. In this context, it can be calculated as

$$E_{CS} = \frac{W(1 - \mu)}{m_{bk}} \quad \text{Eqn. 21}$$

yielding a specific comminution energy in kWh/kg of ore. The reversal of the mass and energy terms is required for this specific energy to accord with the E_{CS} term used in the t_{10} function.

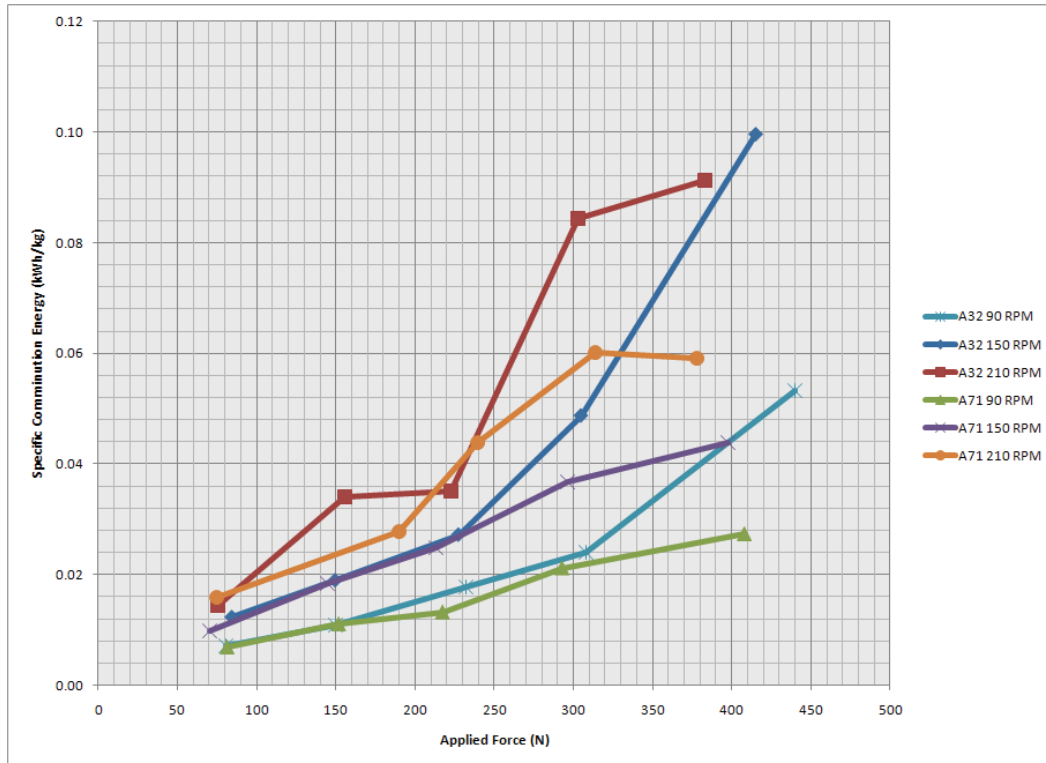


Figure 4-15: Specific comminution energy as a function of applied force, 1018 steel

Plotting the specific comminution energy against the applied force for the 1018 steel system, as seen in Figure 4-15, is the next step. In Figure 4-15, we can see that the specific comminution energy increases with increasing applied force. A high specific comminution energy means that it requires more energy to break a given mass of abrasive. As E_{CS} increases, while the total work input into the system also increases, it becomes less effective at inducing particle breakage. This is consistent with known comminution behaviour, where as the energy input into comminution increases, the rate at which breakage increased diminishes, for a lower rate of return on energy input [21]. In this system, the 90 RPM series have lower specific comminution energy, followed by the 150 RPM, and the 210 RPM having the highest E_{CS} values. This means that the 90 RPM is more effective at

inducing breakage, on a per energy input basis, than the other speeds. This is not to say that the total amount of breakage is higher, but the efficient application of energy is higher. There are two potential reasons for the higher levels of specific comminution energy. First, as with the specific abrasion energy, the work and friction terms are torque dependent, such that the work levels increase rapidly with increasing torque. Increasing the work will increase the E_{CS} value. Second, the breakage mass term for most systems holds relatively steady within a given force range, meaning that the same amount of abrasive is broken, regardless of energy, due to abrasive bypass. Of the amount of material directed at the abrasion interface of the SWAT, approximately a quarter is broken. The amount of abrasive broken is limited by the geometry of the wheel/sample interface, where only a certain percentage of abrasive will pass in the interface and the rest will be ejected to the side as bypass material. Breakage can only occur in material going through the interface. Furthermore, this E_{CS} methodology does not account for the degree of breakage that occurs, that is, the size of the product generated. Looking at the size distribution of the generated material explains a portion of what is occurring. In the tests with the coarse abrasive, a much higher degree of breakage is occurring, as can be seen in Figure 4-16. While the mass of breakage is substantially similar, the degree of breakage is much higher in the Barco 32 than in the Barco 71. This holds true for the other systems studied during the course of this research.

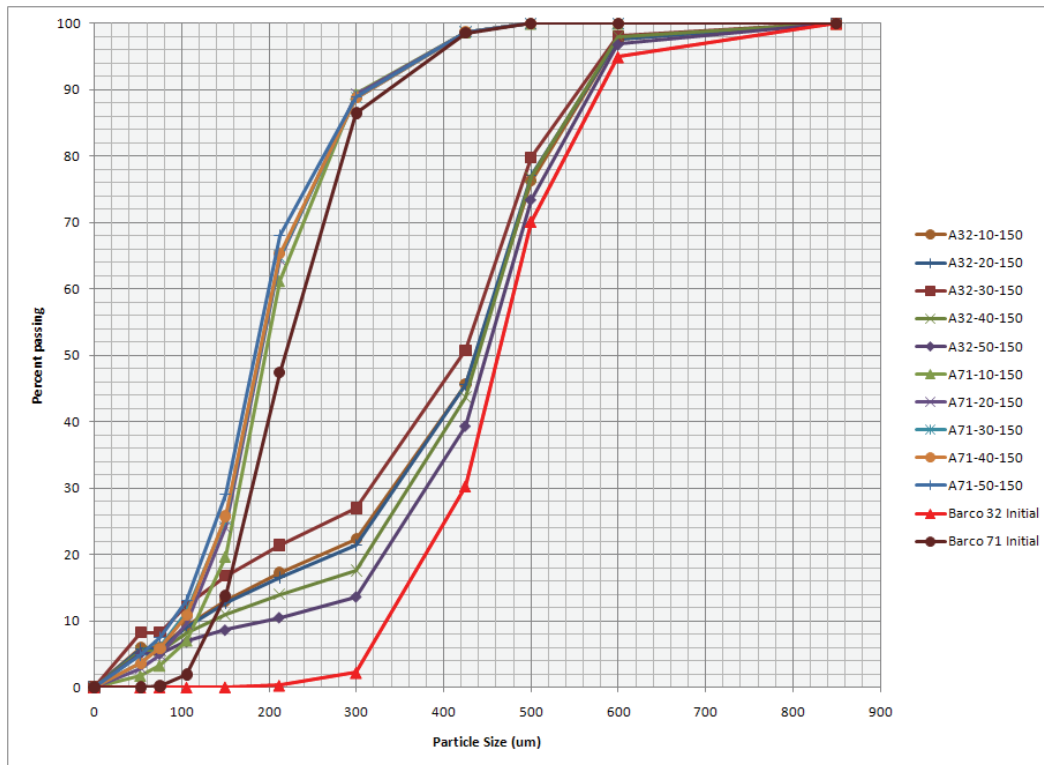


Figure 4-16: Percent passing a given particle size, 1018 steel, 150 RPM

This difference, visible in Figure 4-16, explains the curious result seen in Figure 4-15, where the specific comminution efficiency for the same metal at the same speed is higher for the coarse abrasive than for the fine abrasive. That is, the energy required to break the coarse abrasive was lower than the energy required to break the fine abrasive. This is a violation of known comminution principles with regards to comminution efficiency in fine and ultrafine grinding as opposed to coarse breakage [1, 7]. As the E_{CS} parameter cannot account for the degree of breakage, it cannot be used to compare comminution efficiency between different size classes. This is a flaw held over from the origin of this index in the t_{10} test, which was elaborated using discrete size classes. However, the specific comminution energy may still be used to compare similarly-sized material, where

the size effect will be mitigated. With this caveat for usage, the specific comminution energy term can be employed for the rest of the experiment.

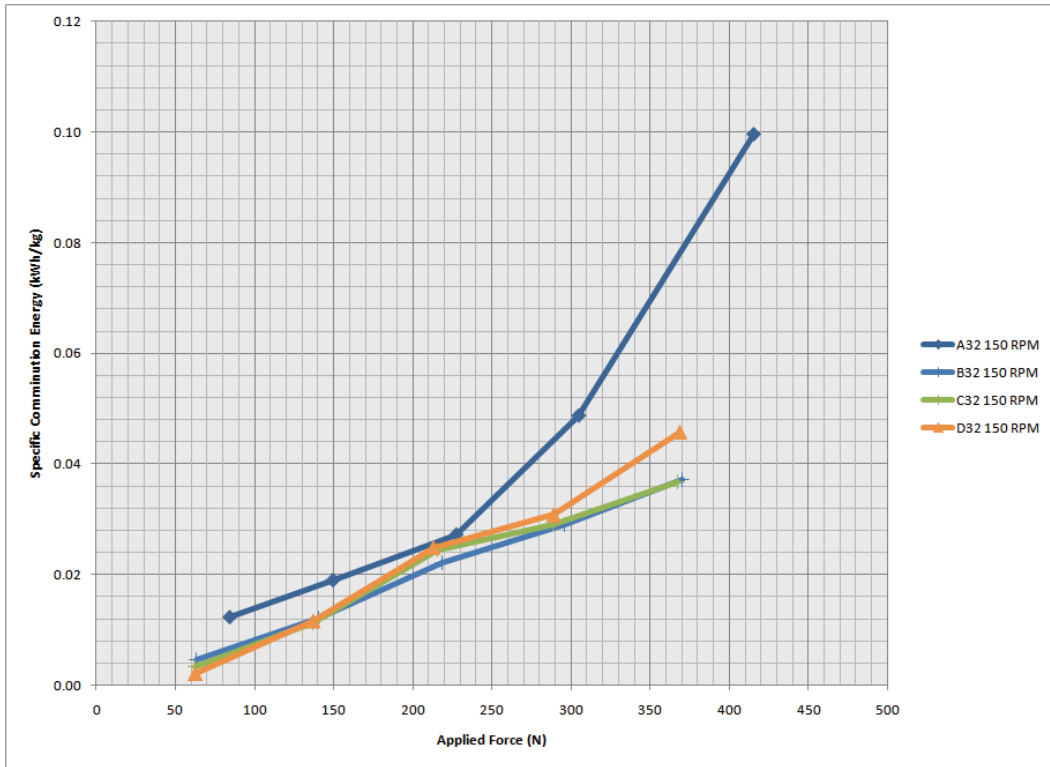


Figure 4-17: Specific comminution energy as a function of applied force, 150 RPM, Barco 32

For all four steel tests, with the same wheel rotational speed, the same trend is seen in Figure 4-17 where the specific comminution energy increases with increasing applied force. The 1018 steel, however, is the only material to exhibit a significant increase in E_{CS} at higher forces. This is once again due to the torque sensitivity of the SWAT results for work and specific energy values. The torque values seen in the 1018 steel tests were much higher than in the 4140, 8620 and 410 tests, as can be seen in Table 4-2.

Table 4-2: Applied force, torque and specific comminution energy, 150 RPM tests

Test	Force (N)	Torque (Nm)	E _{CS} (kWh/kg)
A32-10-150	84.39	6.27	0.012
A32-20-150	149.58	7.73	0.019
A32-30-150	227.47	12.37	0.027
A32-40-150	304.77	16.86	0.049
A32-50-150	415.24	29.68	0.100
B32-10-150	63.27	0.97	0.005
B32-20-150	140.56	5.46	0.012
B32-30-150	218.69	10.16	0.022
B32-40-150	295.58	14.55	0.029
B32-50-150	370.50	18.45	0.037
C32-10-150	62.30	0.73	0.003
C32-20-150	136.56	4.46	0.011
C32-30-150	215.92	9.46	0.025
C32-40-150	288.44	12.76	0.029
C32-50-150	367.59	17.72	0.037
D32-10-150	62.73	0.83	0.002
D32-20-150	137.24	4.63	0.012
D32-30-150	213.07	8.75	0.025
D32-40-150	288.99	12.90	0.031
D32-50-150	368.71	18.00	0.046

The torque in the 1018 steel series is much higher than in the other systems, inducing higher forces, due to the force adjustment parameter seen in Eqn. 15. This can explain some of the excess value of the specific comminution energy. The other tests, with similar force and torque values, have similar specific comminution energy values. The other three steels behave nearly identically.

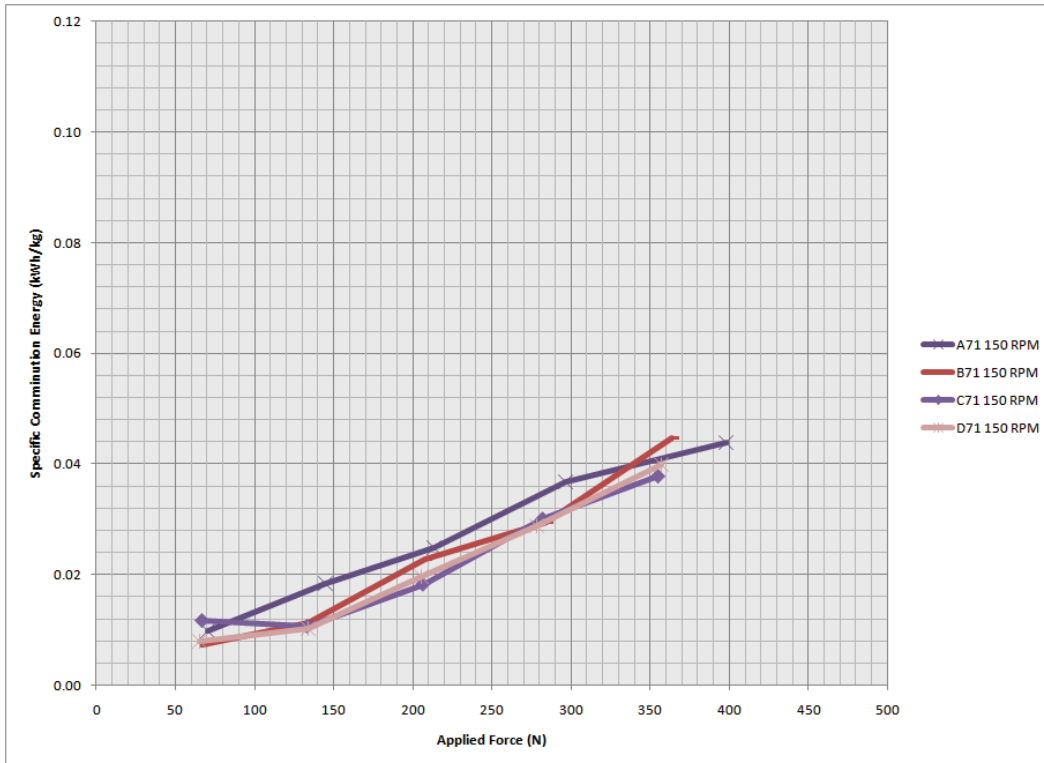


Figure 4-18: Specific comminution energy as a function of applied force, 150 RPM, Barco 71

In the tests with the fine abrasives, the results are much closer. Once again, the specific comminution energy increases with increasing force. All four metal samples behave similarly, with the 1018 steel having a slightly higher E_{CS} value than the other steels, for a given force, in most cases.

4.5 Linking comminution and abrasion specific energies

Having developed two indices to describe the energy distribution during the process, it remains to be seen if these indices can be linked in some manner. Plotting the specific wear energy against the specific comminution energy yields Figure 4-19 and Figure 4-20.

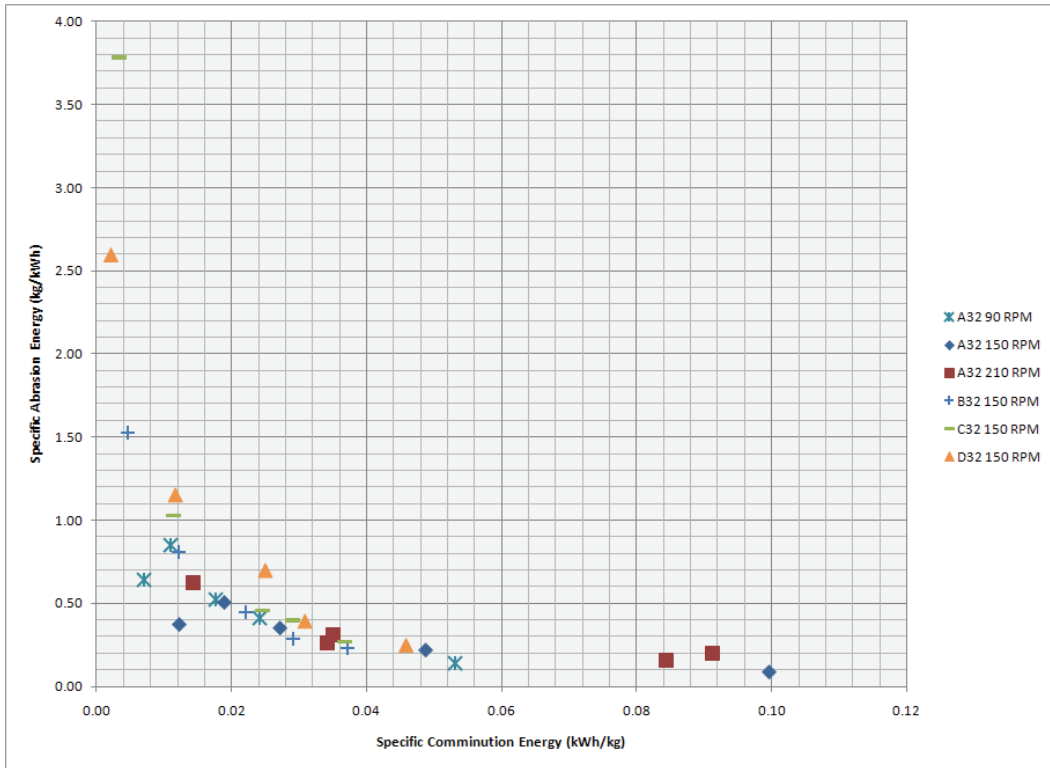


Figure 4-19: Specific comminution energy vs. specific abrasion energy, Barco 32

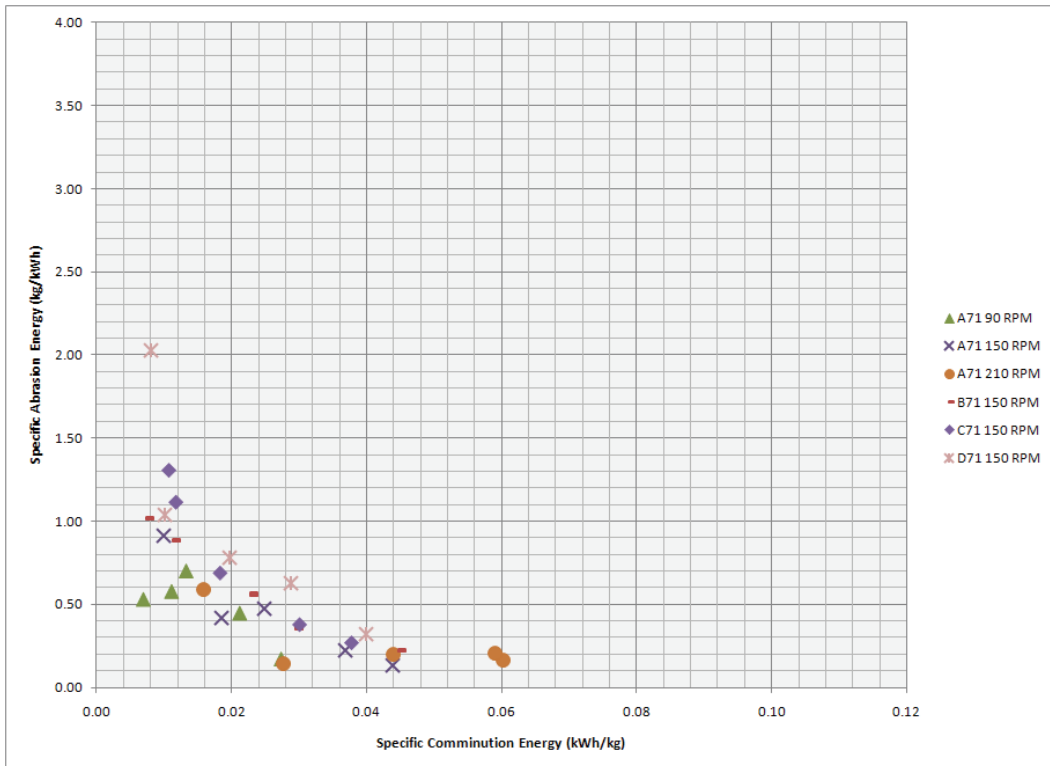


Figure 4-20: Specific comminution energy vs. specific abrasion energy, Barco 71

These figures show an interesting profile, with an inverse relation, where high values of E_{AS} have low values of E_{CS} , and high E_{CS} values have low E_{AS} values. As discussed previously, high specific comminution energy values indicate a less efficient comminution process, while high specific abrasion energy values indicate a more efficient abrasion process. Figure 4-19 and Figure 4-20 seem to indicate that in the energy distribution of the steel wheel abrasion test, specific energy is distributed in such a manner that high specific energy in one process, either abrasion or comminution, will result in a low specific energy in the other process, and vice versa. When a system operates in high specific comminution energy levels, it cannot sustain high specific abrasion energy. The SWAT system can therefore operate in three potential specific energy regimes, shown below.

Table 4-3: Specific energy potential schema

Region	E_{AS} (kWh/kg)	E_{CS} (kWh/kg)	Wear mass loss response	Ore breakage
Lower left	Low	Low	Low	High
Lower right	Low	High	Low	Low
Upper left	High	Low	High	High

By altering system settings, it may be possible to adjust the conditions to investigate a system in a specific regime.

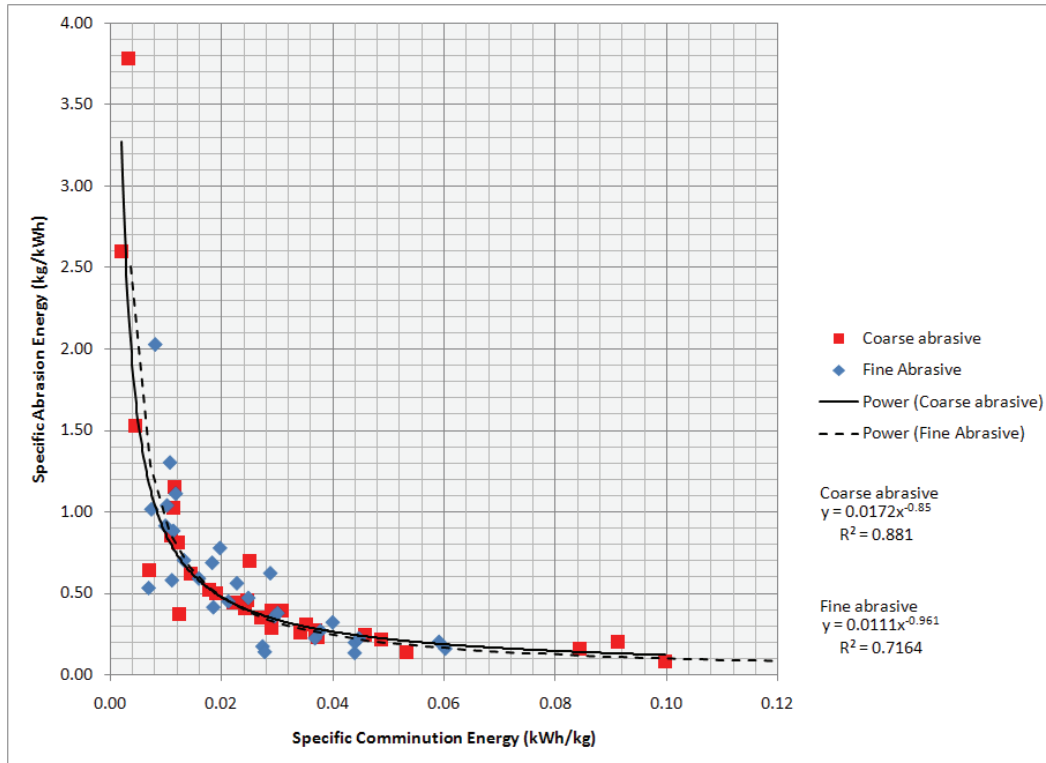


Figure 4-21: Specific comminution energy vs. specific abrasion energy, curve fitting

The specific comminution energy and the specific abrasion energy shown in Figure 4-19 and Figure 4-20 can be plotted together and then curve fitted to a power function of the form

$$f(x) = cx^a \quad \text{Eqn. 22}$$

where c is the scaling factor and a is the exponent. For both the coarse and fine abrasives, the power functions are close to each other. This close link between the two systems is interesting. It seems possible that given one of the specific energy values for a test, the other specific energy value could be calculated. Due to the time-intensive nature of obtaining the specific comminution energy, this relation is particularly interesting. It might be possible to calculate a value of specific

comminution energy without having to measure the abrasive particle breakage, which would greatly accelerate abrasion test work.

4.6 Effect of wheel rotational speed

The tests carried out on the 1018 steel studied the effect of wheel rotational speed on the abrasion and comminution responses. Higher wheel speeds induce higher work on the sample surface. This results, naturally, in higher amounts of absolute wear as mass loss and abrasive breakage. However, the specific energy values are different. Higher speeds induce lower E_{AS} values, indicating that the abrasion process is less efficient. Higher speeds also result in higher E_{CS} levels, indicating less efficient comminution, on a per energy basis. Furthermore, surface analysis, as discussed in section 4.6, shows that at higher speeds the wear regime changes from three-body wear to two-body wear, with direct metal-on-metal contact. This is undesirable in the context of the present research and produces uneven wear scars.

4.7 Analysis of material type performance

Any analysis of different material performance in the present research must address the differences in wear response between the four different steel types employed. The first element of notice is the difference between the 1018 steel and the other three types. To a large degree, the difference between these samples can be linked to the significantly higher torque values seen in the 1018 steels. The torque performance can be divided into two groups, the 1018 by itself,

and the 4140, 8620 and 410 together. This is most likely caused by the damage which occurred in the SWAT coupling systems. It has been seen in most tribological measurement systems that they are very sensitive to any variations in test conditions [22, 47]. Partway through the sets of experiments, damage to the drive shaft coupling required the full removal of the drive shaft, removal of the affected section and machining of a new keyway. The shaft was reinstalled, realigned and adjusted. However, it is impossible to guarantee that the system alignment was identical to the undamaged setting. Modifications in systems response were unavoidable, which means that absolute comparisons between the measured torque values cannot be carried out between the 1018 steel and the other three steel types with absolute confidence.

Comparisons can be run between the 4140, 8620 and 410 steels, however, as they were all measured after the repairs. Figure 4-9 and Figure 4-10, back on page 66, show these results. In terms of absolute wear, for the coarse abrasive seen in Figure 4-9, the 410 stainless had the highest wear overall, the 4140 had a middling performance at low force levels, while 8620 had the best performance at low force levels, switching with the 4140 after 250 N, where the 4140 had the best performance. With the fine abrasive, seen in Figure 4-10, the 4140 had the best performance overall, with the 8620 in a close second and the 410 stainless once again having the highest wear. The specific abrasion energy measurements also sustain these same performance rankings. This can be tied back in part to the hardness values measured for these steels, seen in Table 3-3. 4140 steel has the highest hardness of the test samples, at 64.4 HRA, while 8620 has a hardness of

51.7 HRA and 410 stainless has a hardness of 50.8 HRA. The highest wear resistance is seen in the harder steels.

Of note is the relatively low hardness of these steel samples, particularly in comparison to other potential steel and iron types as encountered in comminution processes. These steels were selected to be representative of general steel classes, but also for commercial availability. Further tests are required to compare with harder steel types and surface treatments, as well as those materials actually in service in the field, preferably from actually tumbling mill charge.

The effect of wheel hardness was another parameter not investigated during the present experiment. The current wheel in service is a plain steel wheel. Further experiments could be carried out, measuring the effect on the wear performance of different counter-surface properties and hardness values.

4.8 Summary

In this chapter, the results of the Steel Wheel Abrasion Test carried out were described and analysed. From these results, the wear behaviour of four steel types was quantified and linked to the abrasive system configuration, influenced by the different applied force loads, abrasive particle size and wheel rotational speeds. Two performance indices were developed and used in results analysis, namely the specific comminution energy, E_{CS} , and the specific abrasion energy, E_{AS} . These two indices were compared to the abrasion test conditions, as well as to each other. This permitted the establishment of a link between both metrics.

Chapter 5 Conclusion

5.1 Conclusion

The goal of the present work was to employ the Steel Wheel Abrasion Test, a laboratory technique used to generate abrasive three-body wear, in the hope that it could be used to simultaneously measure abrasion and comminution. It is desired to link these two processes together, so that the influence of abrasive wear on comminution equipment can be better understood and ultimately reduced. For this, certain goals were laid out for achievement:

1. Develop an understating of the process of comminution.
2. Develop an understating of wear and its component mechanisms.
3. Study the technique by which both of these processes can be replicated and measured effectively.
4. Develop metrics to measure the energy requirements of these processes.
5. Link these energy metrics, to find a connection between abrasive wear and comminution.

To achieve the desired goals, several tasks needed to be accomplished. The processes of comminution and abrasion were first studied in the technical and scientific literature, to understand the metallurgical and mechanical interactions occurring in these processes and their effects. Comminution was studied with regard to the mechanical forces causing particle breakage, as well as the equipment used. Wear was examined, as were the component mechanisms that result in wear. Abrasion was then studied in further detail, both in terms of mechanisms and with regards to modelling and measurement. Using one of these measurement techniques, the Steel Wheel Abrasion Test, abrasive three-body

wear was induced into the surface of steel samples with silica sand. The abrasion response of the material was evaluated, measured and quantified. The particle breakage occurring in the abrasive material was also measured and analysed. It was shown that abrasion and comminution could be studied concurrently using the SWAT. By evaluating the mass loss of the wear sample, as well as the work input into the tribological interaction occurring at the abrasion interface, it was possible to develop the specific abrasion energy, E_{AS} . This term can be used to evaluate the energy expended in abrasion in a material, to develop an abrasion performance index. Furthermore, using the same principle, a comminution index was also deployed, the specific comminution energy, E_{CS} . This term can be used to evaluate the work invested into comminution, and the effectiveness of this work on particle breakage. Upon investigation, it was found that a link could be established between these two metrics, the specific comminution energy and the specific abrasion energy. The specific comminution energy was found to be inversely proportional to the specific abrasion energy, for all systems studied. By linking these two metrics, it is possible to relate the processes of abrasion and comminution. It was found that E_{CS} and E_{AS} could be related together, and fitted to power functions, as shown in Figure 4-21. It was seen that both the fine abrasive Barco 71, and the coarse abrasive, Barco 32, could be fitted to closely related power curves. Given this approximate model, it becomes possible to calculate the value of one specific energy, either abrasion or comminution, given the other. A connection is therefore established between the abrasion and comminution energy metrics

5.2 Recommendations

From the accumulated experience acquired during the course of this work, several suggestions can be made on modifications to experimental parameters, equipment setup and indices development. The following is a listing of some of the more important recommendations arising from the present work, both in recommended future experiments on the current apparatus, as well as design recommendations for the next version of the SWAT.

In terms of future experiments, the materials and conditions used in this experimental work need to be expanded. The current results were collected using four relatively common steels. Other work has been carried out, on older versions of the SWAT procedure and with other parameters, but not for the most recent ones. This test should be expanded to other material types, such as very hard steels and cast irons. It would also be of great interest to test samples taken directly from media used in comminution mills and carry out comparisons with industrial performance. Wheel materials could also be changed, to observe the effect of wheel composition on the abrasive response of the system. The parameters used in the test could also be expanded. The force regime studied is still quite low, when compared to the potential applied force the SWAT is capable of generating. Higher forces could be tested, to see if observed behaviour continues with increasing force. It is recommended that wheel speed be maintained at 150 RPM or below. It has been clearly demonstrated that at higher speeds, the abrasion interaction enters the two-body wear regime, which is not the

purpose of this thesis. Maintaining lower speeds will help ensure that the abrasion occurring is definitely in the three-body regime.

Concerning the abrasives employed in the test, several other recommendations can be made. For general testing, it is believed that standard tests should be carried out with Barco 71, the finer abrasive, rather than with the coarser Barco 32. While both abrasives generate acceptable wear scars, the Barco 71 generates cleaner, more even scars free of the channelling seen in Barco 32. Furthermore, Barco 71 has significantly less traces of two-body wear left behind in the scar. While this abrasive is somewhat more difficult to handle and screen, the improved results justify the switch in the standard test procedure. Barco 71 is also closer in specification to the standard abrasive specified in ASTM G65, the source procedure for our own. It may also be of interest to study different abrasives, both in size and composition, to see if changes in abrasive morphology, composition or mineralogy alter their specific comminution energy results, and how this relates to their abrasivity.

Regardless of which abrasive size is employed, it remains a fact that the specific comminution energy is a size-dependant index, shown to vary with the size of the particles tested. To properly evaluate any abrasive, or to make comparisons between different systems, this size effect must be considered. Furthermore, the current E_{CS} parameter also fails to take into account the degree of breakage occurring in the comminution event. It simply relays the mass of the broken material, not the particle size change. It is recommended that the specific comminution energy term methodology be further reviewed to account for the

size-dependency and the degree of breakage. If the particle size-dependency could be accounted for, then the specific comminution energy could be used to effectively compare breakage between different size classes, which is a limit of the current methodology, due to the test origins, as was discussed when analysing Figure 4-16.

Finally, some recommendations can be made to the intrinsic design of the SWAT apparatus itself. It is first recommended that the linkage between the motor unit and the drive shaft be altered with the current key lock being replaced with a more secure splined shaft. It would remove the potential for failure in that junction, which would have saved the author the non-negligible amount of time and effort needed to make right. In any new machine, the position of the lever arm pivot point needs to be altered. The current machine was designed using an older version of ASTM G65, where the action of the wheel on the sample creates a moment on the sample. This occurs when the surface of the wear sample is not aligned with the arm pivot point. The most recent version of ASTM G65 considers this and describes proper lever arm design [43]. This should be incorporated into any new system, to reduce the influence of torque on the SWAT and simplify the apparatus free body diagram.

With regards to instrumentation, two recommendations can be made. The first is that the current torque gauge on the shaft be upgraded to a more modern torque data acquisition system, from the same supplier. Current sensor technology has been improved over the sensor in present use. It would provide a more reliable torque reading with a better signal and more data parameters. The switch

to an inductively-charged wireless system would also greatly simplify operation. Second, it is recommended that a load cell be incorporated into the system design. The use of a load cell on the wear sample would also be interesting, as it would permit dynamic, real-time measurement of the force applied on the sample, which is impossible in the current generation of test apparatus. This real-time measurement would be ideal for developing more accurate indices due to more accurate force readings.

5.3 Final statement

It has been the objective of the work conducted for this thesis to develop a link between abrasive wear and comminution. From this, it is hoped that a better understanding of the nature of abrasive three-body, high-stress wear, one of the key material degradation processes in comminution equipment, will lead to means of mitigating this wear. It is impossible to totally remove abrasive wear in these systems, as the forces required for comminution are such that wear will always occur in some manner. However, if the processes can be measured, quantified and replicated, then they can be understood and controlled. With this control comes better properties, improved processes and greater efficiency, which are the ultimate goals in proper engineering.

References

1. Fuerstenau, M.C. and K.N. Han, *Principles of mineral processing*. 2003, Littleton, Colo.: Society for Mining, Metallurgy, and Exploration. x, 573 p.
2. Balaz, P., *Mechanochemistry in nanoscience and minerals engineering*. 1.ed.08th ed. 2008, New York, NY: Springer Berlin Heidelberg.
3. Coulson, J.M. and J.F. Richardson, *Coulson & Richardson's chemical engineering*. 1996, Oxford ; Boston: Butterworth-Heinemann. v.
4. Weiss, N.L. and Society of Mining Engineers of AIME., *SME mineral processing handbook*. S. W. Mudd series. 1985, New York: Society of Mining Engineers of the American Institute of Mining, Metallurgical and Petroleum Engineers, Inc.
5. Pascheto, W. and N. Behnood, *Material Testing and Evaluation for Wear Application*, in *International symposium on corrosion and wear of metals*, M. Elboudjaini, G.Y. Lai, and V.S. Sastri, Editors. 1997, Metallurgical Society of CIM: Sudbury, Ontario, Canada.
6. Hertzberg, R.W., *Deformation and fracture mechanics of engineering materials*. 4th ed. 1996, New York: J. Wiley. xxiv, 786 p.
7. Wang, Y. and E. Forssberg, *Enhancement of energy efficiency for mechanical production of fine and ultra-fine particles in comminution*. *China Particuology*, 2007. **5**(3): p. 193-201.
8. Radziszewski, P., et al., *Tumbling mill steel media abrasion wear test development*. *Minerals Engineering*, 2005. **18**(3): p. 333-341.
9. Mishra, B.K., *A review of computer simulation of tumbling mills by the discrete element method: Part I--contact mechanics*. *International Journal of Mineral Processing*, 2003. **71**(1-4): p. 73-93.
10. Morrison, R.D. and P.W. Cleary, *Towards a virtual comminution machine*. *Minerals Engineering*, 2008. **21**(11): p. 770-781.
11. Radziszewski, P., *Exploring total media wear*. *Minerals Engineering*, 2002. **15**(12): p. 1073-1087.
12. Gates, J.D., et al., *The meaning of high stress abrasion and its application in white cast irons*. *Wear*, 2007. **263**(1-6 SPEC. ISS.): p. 6-35.
13. Callister, W.D., *Materials science and engineering : an introduction*. 6th ed. 2003, New York, NY: John Wiley & Sons. xxi, 820 p.

14. Milligan, J., R. Vintila, and M. Brochu, *Nanocrystalline eutectic Al-Si alloy produced by cryomilling*. Materials Science and Engineering A, 2009. **508**(1-2): p. 43-49.
15. Witkin, D.B. and E.J. Lavernia, *Synthesis and mechanical behavior of nanostructured materials via cryomilling*. Progress in Materials Science, 2006. **51**(1): p. 1-60.
16. Gupta, A. and D.S. Yan, *Mineral processing design and operations : an introduction*. 1st ed. 2006, Amsterdam ; Boston: Elsevier. xxiii, 693 p.
17. Perry, R.H., D.W. Green, and J.O. Maloney, *Perry's chemical engineers' handbook*. 7th ed. 2001, New York: McGraw-Hill.
18. Kawatra, S.K., *Advances in comminution*. 2006, Littleton, Colo.: Society for Mining, Metallurgy, and Exploration. vii, 557 p.
19. King, R.P., *Modeling and simulation of mineral processing systems*. 2001, Boston ; Oxford: Butterworth-Heinemann. ix, 403 p.
20. Hewitt, D., *Exploring ore grindability tests with the steel wheel abrasion test (SWAT) machine*. 2009. p. 83 leaves.
21. Olivas, V., *Investigating the use of the steel wheel abrasion test for ore characterization*, in *McGill theses*. 2009.
22. Bhushan, B., *Introduction to tribology*. 2002, New York: John Wiley & Sons. xix, 732 p.
23. Williams, J.A., *Engineering tribology*. 2005, New York: Cambridge University Press. xix, 488 p.
24. Batchelor, A.W., L. Loh Nee, and M. Chandrasekaran, *Materials degradation and its control by surface engineering*. 2nd ed. 2002, London: Imperial College Press. xv, 412 p.
25. Davis, J.R. and Knovel (Firm), *Surface engineering for corrosion and wear resistance*. 2001, Materials Park, OH: ASM International : Institute of Materials. viii, 279 p.
26. Hokkirigawa, K. and K. Kato, *An experimental and theoretical investigation of ploughing, cutting and wedge formation during abrasive wear*. Tribology International, 1988. **21**(1): p. 51-57.
27. Misra, A. and I. Finnie, *A classification of three-body abrasive wear and design of a new tester*. Wear, 1980. **60**(1): p. 111-121.

28. Chenje, T.W., *Development and validation of a model for steel grinding media wear in tumbling mills*. 2007. p. xxi, 216 leaves.
29. Chacon-Nava, J.G., et al., *Some remarks on particle size effects on the abrasion of a range of Fe based alloys*. Tribology International, 2009. **43**(8): p. 1307-1317.
30. Gore, G.J. and J.D. Gates, *Effect of hardness on three very different forms of wear*. Wear, 1997. **203-204**: p. 544-563.
31. Chattopadhyay, R., *Surface wear : analysis, treatment, and prevention*. 2001, Materials Park, OH: ASM International. xii, 307 p.
32. Budinski, K.G., *Guide to friction, wear and erosion testing*. 2007, West Conshohocken, PA: ASTM International. xi, 132 p.
33. Wirojanupatump, S. and P.H. Shipway, *Abrasion of mild steel in wet and dry conditions with the rubber and steel wheel abrasion apparatus*. Wear, 2000. **239**(1): p. 91-101.
34. Dube, N.B. and I.M. Hutchings, *Influence of particle fracture in the high-stress and low-stress abrasive wear of steel*. Wear, 1999. **233-235**: p. 246-256.
35. Torrance, A.A., *The effect of grit size and asperity blunting on abrasive wear*. Wear, 2002. **253**(7-8): p. 813-819.
36. Ala-Kleme, S., et al., *Abrasive wear properties of tool steel matrix composites in rubber wheel abrasion test and laboratory cone crusher experiments*. Wear, 2007. **263**(1-6): p. 180-187.
37. Rabinowicz, E., *Friction and wear of materials*. 2nd ed. 1996, New York: Wiley. xv, 315 p.
38. Rabinowicz, E., L.A. Dunn, and P.G. Russell, *A study of abrasive wear under three-body conditions*. Wear, 1961. **4**(5): p. 345-355.
39. Radziszewski, P., *The steel wheel abrasion test (SWAT): A tool to study wear, friction and ore breakage in the mining industry*. Wear, 2009. **267**(1-4): p. 92-98.
40. *G132-96 Standard Test Method for Pin Abrasion Testing*. Book of standards 03.02. 2006: ASTM International.
41. Sahin, Y., *Optimal testing parameters on the wear behaviour of various steels*. Materials and Design, 2006. **27**(6): p. 455-460.

42. Terva, J., et al., *Abrasive wear of steel against gravel with different rock-steel combinations*. *Wear*, 2009. **267**(11): p. 1821-1831.
43. *G65-04 Standard Test Method for Measuring Abrasion Resistance Using the Dry Sand/Rubber Wheel Apparatus*. Book of standards 03.02. 2006: ASTM International. 245-256.
44. Nahvi, S.M., P.H. Shipway, and D.G. McCartney, *Particle motion and modes of wear in the dry sand-rubber wheel abrasion test*. *Wear*, 2009. **267**(11): p. 2083-2091.
45. Badisch, E., et al., *The comparison of wear properties of different Fe-based hardfacing alloys in four kinds of testing methods*. *Tribo Test*, 2008. **14**(4): p. 225-233.
46. Stevenson, A.N.J. and I.M. Hutchings, *Development of the dry sand/rubber wheel abrasion test*. *Wear*, 1996. **195**(1-2): p. 232-240.
47. Stachowiak, G.W., A.W. Batchelor, and G. Stachowiak, *Experimental methods in tribology*. 1st ed. Tribology series. 2004, Amsterdam, The Netherlands ; San Diego, CA: Elsevier. xviii, 354 p.
48. Natarajan, K.A., *Laboratory studies on ball wear in the grinding of a chalcopyrite ore*. *International Journal of Mineral Processing*, 1996. **46**(3-4): p. 205-213.
49. Gates, J.D., et al., *Effect of abrasive mineral on alloy performance in the ball mill abrasion test*. *Wear*, 2008. **265**(5-6): p. 865-870.
50. Chenje, T.W., D.J. Simbi, and E. Navara, *The role of corrosive wear during laboratory milling*. *Minerals Engineering*, 2003. **16**(7): p. 619-624.
51. Chenje, T.W., D.J. Simbi, and E. Navara, *Relationship between microstructure, hardness, impact toughness and wear performance of selected grinding media for mineral ore milling operations*. *Materials and Design*, 2004. **25**(1): p. 11-18.
52. Radziszewski, P., *Developing an experimental procedure for charge media wear prediction*. *Minerals Engineering*, 2000. **13**(8-9): p. 949-961.
53. Banisi, S. and M. Hadizadeh, *3-D liner wear profile measurement and analysis in industrial SAG mills*. *Minerals Engineering*, 2007. **20**(2): p. 132-139.
54. Cleary, P.W., *Recent advances in DEM modelling of tumbling mills*. *Minerals Engineering*, 2001. **14**(10): p. 1295-1319.

55. Rezaeizadeh, M., et al., *A new predictive model of lifter bar wear in mills*. Minerals Engineering, 2010. **23**(15): p. 1174-1181.
56. Hosseini, P., *Exploring energy usage in comminution and media wear using steel wheel abrasion test* 2010. p. xxi, 105 leaves.
57. *Material Safety Data Sheet: Silica Sand*. 2006, Opta Minerals: Waterdown, ON. p. 6.
58. *Quartz*, in *The Columbia Encyclopedia*. 2008, Columbia University Press.
59. Perkins, D., *Mineralogy*. 2nd ed. 2002, Upper Saddle River, N.J.: Prentice Hall. xii, 483 p.
60. Davis, J.R. and ASM International. Handbook Committee., *Carbon and alloy steels*. ASM speciality handbook. 1996, Materials Park, OH: ASM International. v, 731 p.
61. Harvey, P.D. and American Society for Metals., *Engineering properties of steel*. 1982, Metals Park, Ohio: American Society for Metals. v, 527 p.
62. Chenje, T.W., J.-P. Lafleur, and P. Hosseini, *Abrasion Tester (SWAT) Operational Procedure*. 2010, Comminution Dynamics Laboratory, McGill University: Montreal, QC. p. 4.
63. Nikas, G.K., *Effects of operating conditions and friction on the entrapment of spherical debris particles in elliptical contacts*. Proceedings of the Institution of Mechanical Engineers, Part J: Journal of Engineering Tribology, 2007. **221**(6): p. 727-741.